

# Tumor immunoevasion by the conversion of effector NK cells into type 1 innate lymphoid cells

Yulong Gao<sup>1,2,18</sup>, Fernando Souza-Fonseca-Guimaraes<sup>1,3,4,18</sup>, Tobias Bald<sup>1</sup>, Susanna S Ng<sup>5,6</sup>, Arabella Young<sup>1,2</sup>, Shin Foong Ngiew<sup>1</sup>, Jai Rautela<sup>3</sup>, Jasmin Straube<sup>7</sup>, Nic Waddell<sup>7</sup>, Stephen J Blake<sup>8</sup>, Juming Yan<sup>2,8</sup>, Laurent Bartholin<sup>9</sup>, Jason S Lee<sup>10</sup>, Eric Vivier<sup>11</sup>, Kazuyoshi Takeda<sup>12</sup>, Meriem Messaoudene<sup>13,14</sup>, Laurence Zitvogel<sup>14–16</sup>, Michele W L Teng<sup>2,8</sup>, Gabrielle T Belz<sup>3</sup>, Christian R Engwerda<sup>5</sup>, Nicholas D Huntington<sup>3</sup>, Kyohei Nakamura<sup>1</sup>, Michael Hölzel<sup>17</sup> & Mark J Smyth<sup>1,2</sup>

Avoiding destruction by immune cells is a hallmark of cancer, yet how tumors ultimately evade control by natural killer (NK) cells remains incompletely defined. Using global transcriptomic and flow-cytometry analyses and genetically engineered mouse models, we identified the cytokine-TGF- $\beta$ -signaling-dependent conversion of NK cells (CD49a-CD49b+Eomes<sup>+</sup>) into intermediate type 1 innate lymphoid cell (intILC1) (CD49a+CD49b+Eomes<sup>+</sup>) populations and ILC1 (CD49a+CD49b-Eomes<sup>int</sup>) populations in the tumor microenvironment. Strikingly, intILC1s and ILC1s were unable to control local tumor growth and metastasis, whereas NK cells favored tumor immunosurveillance. Experiments with an antibody that neutralizes the cytokine TNF suggested that escape from the innate immune system was partially mediated by TNF-producing ILC1s. Our findings provide new insight into the plasticity of group 1 ILCs in the tumor microenvironment and suggest that the TGF- $\beta$ -driven conversion of NK cells into ILC1s is a previously unknown mechanism by which tumors escape surveillance by the innate immune system.

Natural killer (NK) cells are critical for controlling tumor initiation and metastasis, and increasing efforts are now being expended to fully exploit the anti-tumor properties of NK cells in the clinic<sup>1</sup>. Cytokines and metabolites reported to directly suppress the anti-tumor properties of NK cells include TGF- $\beta$ . It is generally viewed as an important immunosuppressive cytokine in the tumor microenvironment<sup>2,3</sup> and can inhibit the activation of NK cells, the expression of cytotoxic proteins and the cytotoxic process by various mechanisms<sup>4–7</sup>. It has been shown that intrinsic TGF- $\beta$  signaling affects the number and anti-metastatic function of NK cells<sup>8</sup>.

Although they phenotypically resemble NK cells, type 1 innate lymphoid cells (ILC1s) develop from a common helper innate lymphoid progenitor cell that gives rise to all members of the ILC family but not NK cells<sup>9,10</sup>. NK cells develop from NK cell precursors and are found predominantly circulating in the blood and within secondary lymphoid tissues, such as the spleen. In contrast, typically ILC1s are not

found in blood or lymphoid organs<sup>11</sup>. In adult mice, liver ILC1s have been well characterized, and they display phenotypic features distinct from those of liver NK cells. Both NK cells and ILC1s in the liver express the transcription factor T-bet; however, liver ILC1s do not express the transcription factor Eomes<sup>11</sup>. Gene-expression profiling and flow cytometry have identified additional molecules expressed differentially by NK cells versus ILC1s<sup>9,12,13</sup>. Group 1 ILCs in mice are defined as lineage-marker-negative (Lin<sup>-</sup>: CD3<sup>-</sup>TCR $\beta$ -CD19<sup>-</sup>) CD45<sup>+</sup>NK1.1<sup>+</sup>NKp46<sup>+</sup> cells, of which two subsets have been identified in the liver so far. Resting mature NK cells are defined in mice as Lin<sup>-</sup> CD45<sup>+</sup>NK1.1<sup>+</sup>NKp46<sup>+</sup>CD49a-CD49b<sup>+</sup> lymphocytes that lack expression of the cytotoxic molecule TRAIL<sup>11</sup>. Liver ILC1s are defined as Lin<sup>-</sup>CD45<sup>+</sup>NK1.1<sup>+</sup>NKp46<sup>+</sup>CD49b<sup>-</sup> cells with high expression of both the integrin CD49a (VLA-1) and TRAIL. Among those, tissue-resident markers such as CD49a support the sentinel-like tissue-resident characteristics of ILC1s.

<sup>1</sup>Immunology in Cancer and Infection, QIMR Berghofer Medical Research Institute, Herston, Queensland, Australia. <sup>2</sup>School of Medicine, The University of Queensland, Herston, Queensland, Australia. <sup>3</sup>Molecular Immunology Division, The Walter and Eliza Hall Institute of Medical Research, Department of Medical Biology and The University of Melbourne, Parkville, Victoria, Australia. <sup>4</sup>Faculty of Medicine, Dentistry and Health Sciences, The University of Melbourne, Melbourne, Victoria, Australia. <sup>5</sup>Immunology and Infection, QIMR Berghofer Medical Research Institute, Herston, Queensland, Australia. <sup>6</sup>School of Natural Sciences, Griffith University, Nathan, Queensland, Australia. <sup>7</sup>Medical Genomics, QIMR Berghofer Medical Research Institute, Herston, Queensland, Australia. <sup>8</sup>Cancer Immunoregulation and Immunotherapy, QIMR Berghofer Medical Research Institute, Herston, Queensland, Australia. <sup>9</sup>Université Claude Bernard Lyon 1, INSERM 1052, CNRS 5286, Centre Léon Bérard, Centre de recherche en cancérologie de Lyon, Lyon, France. <sup>10</sup>Control of Gene Expression Laboratory, QIMR Berghofer Medical Research Institute, Herston, Queensland, Australia. <sup>11</sup>Centre d'Immunologie de Marseille-Luminy, Aix Marseille Université, INSERM, CNRS, Marseille, France. <sup>12</sup>Division of Cell Biology, Biomedical Research Center and Department of Biofunctional Microbiota, Graduate School of Medicine, Juntendo University, Bunkyo-ku, Tokyo, Japan. <sup>13</sup>INSERM U1015, Gustave Roussy Cancer Campus, Villejuif, France. <sup>14</sup>Gustave Roussy Cancer Campus, Villejuif, France. <sup>15</sup>University Paris-Saclay, Kremlin Bicêtre, Paris, France. <sup>16</sup>CIC1428, Gustave Roussy Cancer Campus, Villejuif, France. <sup>17</sup>Unit for RNA Biology, Department of Clinical Chemistry and Clinical Pharmacology, University of Bonn, Bonn, Germany. <sup>18</sup>These authors contributed equally to this work. Correspondence should be addressed to M.J.S. (mark.smyth@qimrberghofer.edu.au).

Received 17 April; accepted 23 June; published online 31 July 2017; doi:10.1038/ni.3800

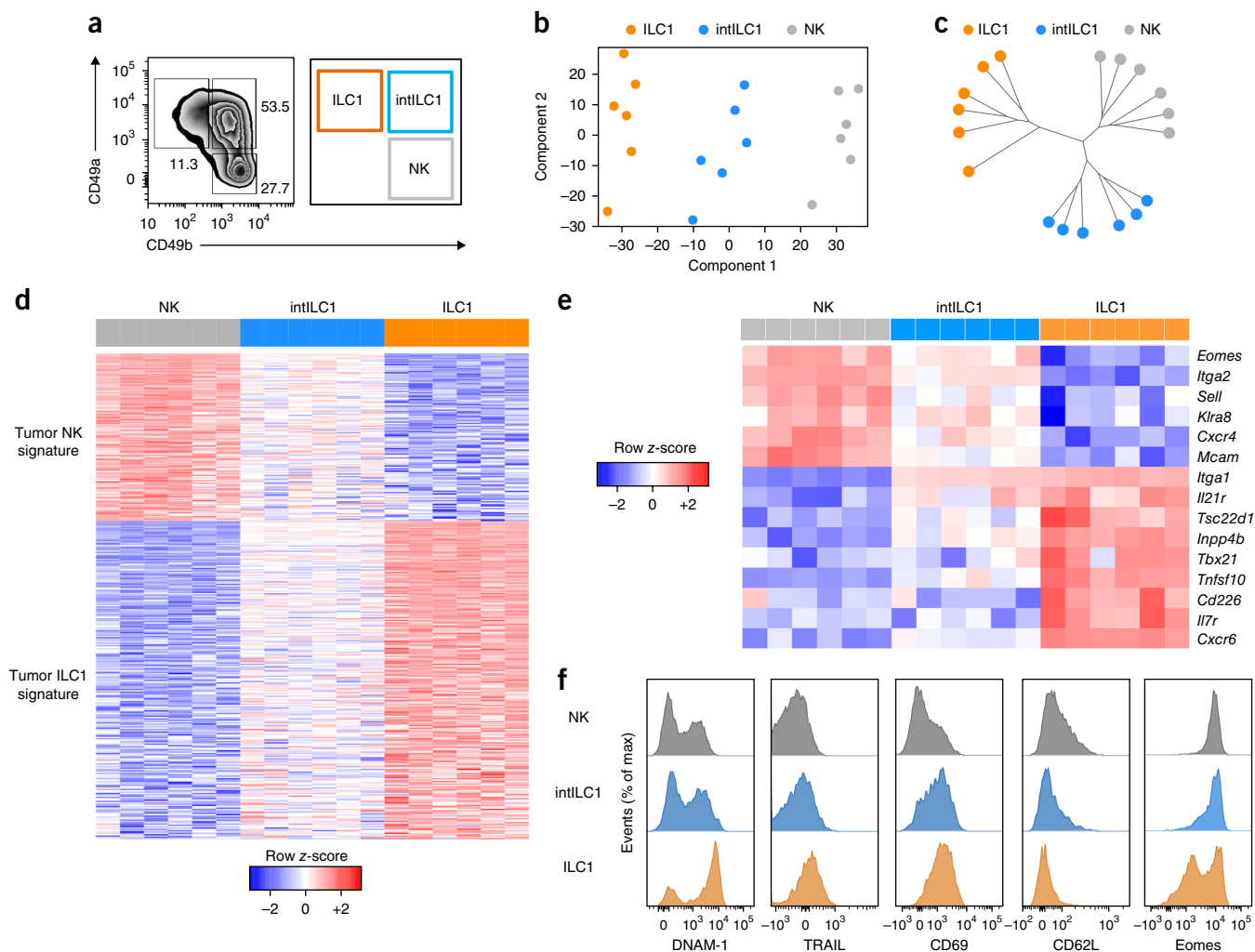


**Figure 1** Three distinct populations of group 1 ILCs infiltrate MCA1956 tumors. **(a)** Flow cytometry (left) of cells from a subcutaneous MCA1956 tumor, showing its group 1 ILC composition. Numbers adjacent to outlined areas (left) indicate percent cells in each subset (identified at right). **(b,c)** Classical multidimensional scaling of six matched triplicates of tumor NK cell, intILC1 and ILC1 populations (key) isolated from the same MCA1956 tumor ( $n = 6$ ) **(b)**, and a phylogenetic tree of a corresponding divisive hierarchical cluster analysis ( $n = 6$  tumors) **(c)**. **(d)** Differential expression of genes (one per row; change of  $>1$ -fold ( $\log_2$  value) and false-discovery rate (FDR) of  $<0.01$ ) in tumor group 1 ILC subsets (above plots; one sample per column), based on gene signatures obtained from tumor NK cells and ILC1s (left margin), presented as row-wise z-scores of  $\log_2$ -transformed normalized RNA-sequencing read counts (key). **(e)** Expression (key; as in **d**) of genes encoding markers of tumor NK cells or ILC1s (right margin) in tumor group 1 ILC subsets (above plots), curated manually. Selected genes and products: *Itga2*, CD49b; *Itga1*, CD49a; *Tbx21*, T-bet; *Tnfsf10*, TRAIL. **(f)** Flow-cytometry analysis of the expression of various markers (horizontal axes) in tumor group 1 ILC subsets ( $n = 6$  tumors). Data are representative of four experiments **(a)** or one experiment **(b–e)** or are from three independent experiments **(f)**.

Strikingly, such tissue residency is maintained even under systemic inflammatory conditions<sup>14</sup>, which raises questions about their homeostatic maintenance and their role in disease conditions such as cancer. Furthermore, despite clear functional and phenotypic similarities between ILCs and NK cells, little is known about any lineage relationships between these cells, which has become an important issue, with published reports questioning their relationship<sup>15–17</sup>. In particular, it is unclear whether, like the myeloid lineage, there might be some plasticity between NK cells and ILCs under pathological conditions, such as tumor development and metastasis. In addition, it remains to be established whether ILCs have any role in the early innate immunosurveillance of cancer or whether this role is performed mainly by tumor-associated NK cells<sup>18,19</sup>. To address these questions, we used primary, transplantable and metastatic cancer models as well as transgenic mice

to investigate the function and phenotypic plasticity of tumor group 1 ILCs.

## RESULTS

### Three subsets of tumor group 1 ILCs

The methylcholanthrene (MCA)-induced fibrosarcoma cell line MCA1956 was transplanted subcutaneously into C57BL/6 mice, and the composition of group 1 ILC subsets was characterized by flow cytometry. Three populations of Lin<sup>−</sup>CD45<sup>+</sup>NK1.1<sup>+</sup>NKp46<sup>+</sup> cells (tumor group 1 ILCs) were identified, which were discriminated by expression of the integrins CD49a and CD49b. MCA1956 tumors were composed of CD49a<sup>+</sup>CD49b<sup>−</sup> ILC1s (~10%) and CD49a<sup>−</sup>CD49b<sup>+</sup> NK cells (~30%) (**Fig. 1a**), but, intriguingly, the largest population of tumor group 1 ILCs (~50%) were CD49a<sup>+</sup>CD49b<sup>+</sup> cells (**Fig. 1a**). We hypothesized that CD49a<sup>+</sup>CD49b<sup>+</sup> cells might be a distinct

population with features of NK cells and ILC1s; thus, we called these CD49a<sup>+</sup>CD49b<sup>+</sup> cells 'intermediate ILC1s' (intILC1s). We next performed global transcriptomic analysis of NK cells, intILC1s and ILC1s isolated from MCA1956 tumors. Classical multidimensional scaling and clustering analysis indicated that the three subsets had distinct gene-expression profiles (Fig. 1b,c and Supplementary Fig. 1a,b). Comparisons revealed various genes that were expressed differentially by NK cells relative to their expression by ILC1s (Fig. 1b,c and Supplementary Fig. 1a,b). Indeed, these analyses substantiated the proposal that CD49a<sup>+</sup>CD49b<sup>+</sup> cells displayed an intermediate phenotype that placed them between tumor NK cells and ILC1s (Fig. 1b,d). Of note, the gene signatures of tumor NK cells and ILC1s substantially correlated with gene-expression data generated from NK cells and ILC1s isolated from the liver or spleen<sup>9</sup> (Supplementary Tables 1 and 2 and Supplementary Fig. 1c,d). We also confirmed the differential expression of genes encoding well-established markers of NK cell and ILC1 in the respective subpopulations<sup>12</sup> (Fig. 1e). Flow cytometry showed that CD49a<sup>+</sup>CD49b<sup>+</sup> intILC1s shared features with both NK cells and ILC1s in the tumor, characterized by lower expression of Eomes and the memory marker CD62L, as well as higher expression of the activation marker CD69 and activating receptor DNAM-1, than that of tumor NK cells (Fig. 1f). Thus, our data suggested that CD49a<sup>+</sup>CD49b<sup>+</sup> intILC1s were distinct from NK cells and ILC1s and had an intermediate phenotype.

### TGF- $\beta$ converts NK cells into ILC1s *in vitro* and *in vivo*

Published studies have substantiated the fact that NK cells can switch their phenotype in response to exogenous mediators such as TGF- $\beta$ <sup>20,21</sup>. Thus, we hypothesized that intILC1s and ILC1s arose from NK cells due to TGF- $\beta$ -induced differentiation. To assess this, we reconstituted immunodeficient (*Rag2*<sup>-/-</sup>) mice lacking expression of the common  $\gamma$ -chain (*Il2rg*<sup>-/-</sup>; called ' $\gamma$ c<sup>-/-</sup>' here) with freshly isolated mature splenic NK cells (Lin<sup>-</sup>CD45<sup>+</sup>NK1.1<sup>+</sup>NKp46<sup>+</sup>CD49a<sup>+</sup>CD49b<sup>+</sup>). At 7 d after reconstitution, NK cell-derived intILC1 and ILC1 populations emerged in host livers; these became more prevalent on day 14 and were maintained at a similar frequency by day 21 (Fig. 2a). Of note, expression of the activating receptor NKp46 (encoded by *Ncr1*) occurs only following the commitment of precursors of NK cells to the NK cell lineage<sup>22</sup>, which excluded the possibility that contamination by precursors of NK cells was responsible for the phenotype observed. The NK cell-derived ILC1s showed a typical liver ILC1 phenotype (for example, TRAIL<sup>+</sup>DNAM-1<sup>+</sup>Eomes<sup>int</sup>), and NK cell-derived intILC1s *ex vivo* were TRAIL<sup>int</sup>DNAM-1<sup>+</sup>Eomes<sup>+</sup> (Fig. 2b). To investigate the role of TGF- $\beta$  signaling in the conversion of NK cells, we used transgenic mice with TGF- $\beta$  signaling that was ablated specifically in NKp46<sup>+</sup> cells (*Ncr1*<sup>cre/wt</sup>*TgfbRII*<sup>fl/fl</sup> mice; called '*RII*<sup>FL</sup>' mice here), along with their corresponding controls (*Ncr1*<sup>wt/wt</sup>*TgfbRII*<sup>fl/fl</sup> mice; called '*RII*<sup>WT</sup>' mice here), and transgenic mice with TGF- $\beta$  signaling that was constitutively active specifically in NKp46<sup>+</sup> cells (*Ncr1*<sup>cre/wt</sup>*TgfbRICA*<sup>fl/fl</sup> mice; called '*RI*<sup>CA-FL</sup>' mice here), and their corresponding controls (*Ncr1*<sup>wt/wt</sup>*TgfbRICA*<sup>fl/fl</sup> mice; called '*RI*<sup>CA-WT</sup>' mice here)<sup>8</sup>. We first assessed whether TGF- $\beta$  altered the homeostasis of ILC1s in these mice. The *RI*<sup>CA-FL</sup> mice had a significantly lower proportion and number of NK cells and a correspondingly higher frequency, but not number, of ILC1s than that of *RI*<sup>CA-WT</sup> mice ( $P < 0.01$ ; Supplementary Fig. 2a-c). Constitutively active TGF- $\beta$  signaling in NKp46<sup>+</sup> cells (in *RI*<sup>CA-FL</sup> mice) significantly diminished the abundance of peripheral NK cells in the liver and spleen (Supplementary Fig. 2a-c) and in the bone marrow and peripheral blood (data not shown), relative to that of *RI*<sup>CA-WT</sup> mice. In contrast, mice with ablated TGF- $\beta$  signaling

in NKp46<sup>+</sup> cells (*RII*<sup>FL</sup> mice) demonstrated a significant reduction in the proportion and number of liver ILC1s relative to that of *RII*<sup>WT</sup> mice ( $P < 0.01$ ; Supplementary Fig. 2a-c). Whereas the majority of the group 1 ILCs were CD49b<sup>+</sup> NK cells in spleen, the liver contained a substantial proportion (~25%) of CD49a<sup>+</sup> ILC1s in littermates of the appropriate control strain (*RI*<sup>CA-WT</sup> or *RII*<sup>WT</sup>) (Supplementary Fig. 2a-c). These results highlighted the hypothesis that TGF- $\beta$  signaling in NKp46<sup>+</sup> cells favored the maintenance of ILC1s.

Next, we isolated splenic NK cells from *RII*<sup>WT</sup> mice and cultured the cells in serum-free medium supplemented with the NK cell-activating cytokine IL-15 and TGF- $\beta$ . We observed that the expression of ILC1-related markers (for example, CD49a, DNAM-1 and TRAIL) was increased and expression of Eomes was downregulated in a TGF- $\beta$ -dose-dependent manner (Fig. 2c and Supplementary Fig. 2d,e). That increased expression was strictly dependent on TGF- $\beta$  signaling, as splenic NK cells isolated from *RII*<sup>FL</sup> mice maintained their NK cell phenotype (Fig. 2c). We next isolated NK cells from the spleen of *RI*<sup>CA-WT</sup> and *RI*<sup>CA-FL</sup> mice and cultured the cells with IL-15. A proportion of NK cells from *RI*<sup>CA-FL</sup> mice converted into intILC1s after 4 d of culture, whereas intILC1 from *RI*<sup>CA-FL</sup> mice failed to convert into ILC1s *in vitro* (Supplementary Fig. 2f,g). Further analysis revealed that ILC1s did not convert into NK cells after stimulation with TGF- $\beta$  *in vitro* (Supplementary Fig. 2h,i). However, intILC1s were able to give rise to ILC1s in the liver 14 d after being transferred into *Rag2*<sup>-/-</sup> $\gamma$ c<sup>-/-</sup> mice (Fig. 2d). Moreover, splenic NK cells isolated from *RII*<sup>FL</sup> mice largely maintained their phenotype, and only a small proportion differentiated into intILC1s and ILC1s in the liver of *Rag2*<sup>-/-</sup> $\gamma$ c<sup>-/-</sup> mice (Fig. 2d). Overall, these results demonstrated the role of TGF- $\beta$  signaling in the conversion of NK cells into intILC1s and ILC1s.

### Increased proliferative activity of intILC1s

Precursor cells proliferate before they acquire a terminal differentiated state, which usually occurs with cell-cycle arrest<sup>23</sup>. Thus, we hypothesized that the conversion of NK cells into ILC1s was initiated by a proliferative response, followed by terminal differentiation. Gene-set-enrichment analyses (GSEA) using the Broad hallmark gene-set collection<sup>24</sup> demonstrated that intILC1s showed significant enrichment for the expression of gene sets encoding cell-cycle-related molecules relative to their expression in ILC1s in tumors (Fig. 3a,c). Detailed transcriptomic analysis showed that tumor intILC1s had the highest expression of gene sets encoding cell-cycle-related molecules, among all tumor group 1 ILC subsets, followed by NK cells and ILC1s (Fig. 3b,d). Cross-comparison of the expression of gene sets encoding cell-cycle-related molecules in liver NK cells and ILC1s substantiated the proposal that proliferation capacity also varied among group 1 ILC subsets in non-tumor tissues (Supplementary Fig. 3). To further assess the proliferation rate of group 1 ILC subsets, we performed an *in vivo* proliferation assay. As described above (Fig. 2a), we reconstituted *Rag2*<sup>-/-</sup> $\gamma$ c<sup>-/-</sup> mice with splenic NK cells (Lin<sup>-</sup>CD45<sup>+</sup>NK1.1<sup>+</sup>NKp46<sup>+</sup>CD49a<sup>+</sup>CD49b<sup>+</sup>) and measured expression of the proliferation marker Ki67 by NK cell-derived ILC1 subsets on days 7 and 14 after reconstitution. On day 7 after transfer, all subsets had substantial Ki67 expression (Fig. 3e). Consistent with our transcriptomic analysis of group 1 ILC subsets isolated from endpoint tumors (Fig. 3a-d), NK cell-derived intILC1s were the most proliferative cells at 14 d after transfer (Fig. 3e). Together these data indicated that the TGF- $\beta$ -driven conversion of tumor NK cells into intILC1s and ILC1s was associated with a transient increase in the proliferation of differentiating intILC1s.

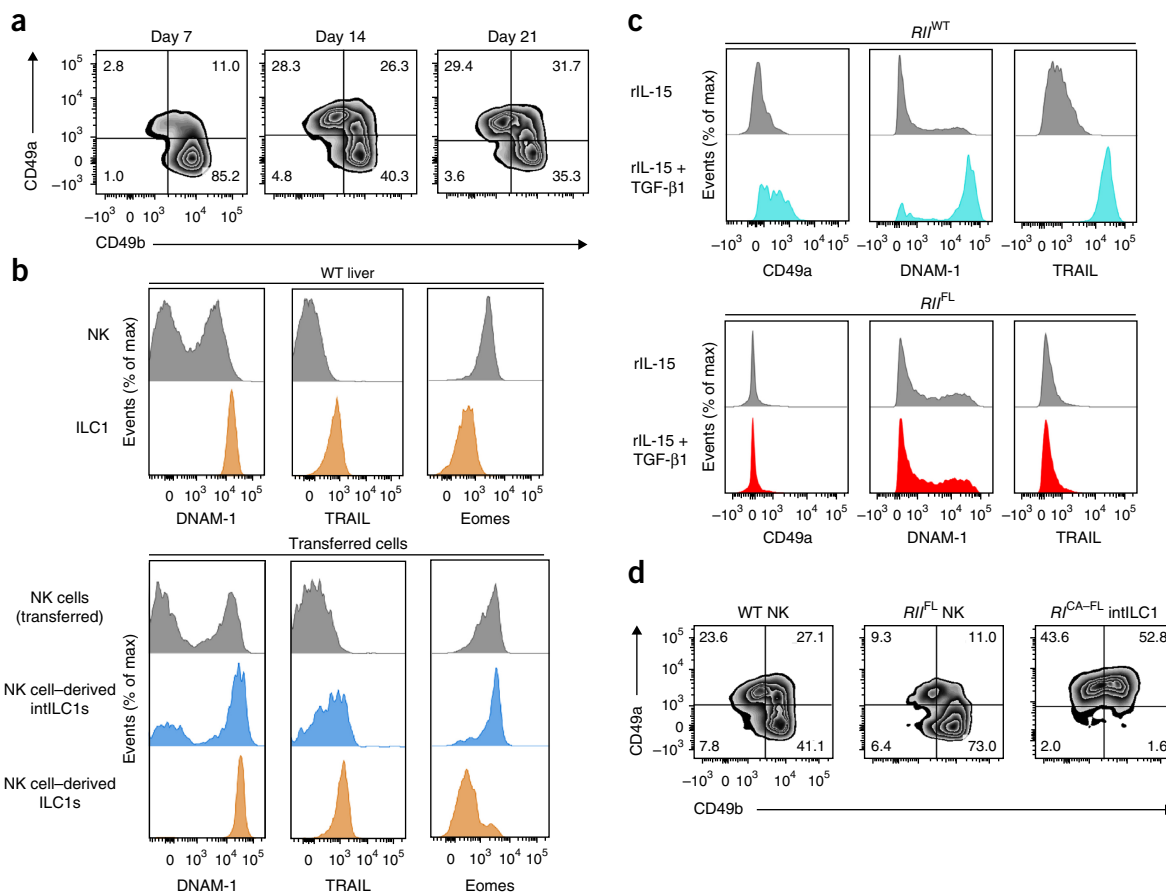


**Figure 2** The conversion of NK cells into ILC1-like cells is dependent on TGF- $\beta$  signaling. **(a)** Flow cytometry of cells obtained from the liver of *Rag2*<sup>-/-</sup> $\gamma$ c<sup>-/-</sup> mice on day 7, 14 or 21 (above plots) after intravenous injection of  $5 \times 10^5$  splenic NK cells purified from wild-type mice, identifying group 1 ILC composition. Numbers in quadrants indicate percent cells in each throughout (quadrants defined as in **Fig. 1a**). **(b)** Flow cytometry of NK cells and ILC1s in the liver of wild-type mice (top group) and NK cell-derived group 1 ILC subsets (left margin) in the liver of *Rag2*<sup>-/-</sup> $\gamma$ c<sup>-/-</sup> mice given adoptive transfer of wild-type splenic NK cells (bottom group), assessing the expression of DNAM-1, TRAIL and Eomes. **(c)** Flow cytometry of splenic NK cells sorted from *RII*<sup>WT</sup> mice (top group) or *RII*<sup>FL</sup> mice (bottom group) and cultured for 5 d in medium containing a complex of recombinant IL-15 (rIL-15) and its receptor IL-15R $\alpha$  (25 ng/ml), alone or supplemented with TGF- $\beta$ 1 (6.25 ng/ml) (left margin), assessing the expression of CD49a, DNAM-1 and TRAIL. **(d)** Flow cytometry of cells from the liver of *Rag2*<sup>-/-</sup> $\gamma$ c<sup>-/-</sup> mice reconstituted with NK cells isolated from the spleen of wild-type mice (left) or *RII*<sup>FL</sup> mice (middle) or intILC1s from spleen of *RII*<sup>CA-FL</sup> mice (right), showing group 1 ILC composition 14 d after cell transfer. Data are representative of three experiments with  $n = 9$  mice (day 7),  $n = 8$  (day 14) or  $n = 4$  (day 21) **(a)**, two experiments with  $n = 8$  mice **(b)** or two experiments with  $n = 3$  mice **(c)** or are from one experiment with  $n = 4$  mice (left and middle) or  $n = 3$  mice (right) **(d)**.

### TGF- $\beta$ drives the conversion of NK cells into ILC1s in tumors

Next we investigated whether the conversion of NK cells also occurred in the tumor microenvironment. We obtained splenic NK cells isolated from *RII*<sup>FL</sup> and *RII*<sup>WT</sup> mice and injected the cells intravenously into MCA1956-tumor-bearing *Rag2*<sup>-/-</sup> $\gamma$ c<sup>-/-</sup> mice (**Fig. 4a**). At 16 d after the transfer of *RII*<sup>WT</sup> NK cells, we observed NK cell-derived intILC1s and ILC1s within the tumor microenvironment (**Fig. 4a,b**). That conversion was significantly lower in tumor-bearing mice reconstituted with splenic NK cells isolated from *RII*<sup>FL</sup> mice than in those reconstituted with such cells from *RII*<sup>WT</sup> mice (**Fig. 4b,c**). Transferred NK cells also converted into intILC1s in MCA1956-tumor-bearing, congenically marked (CD45.1<sup>+</sup>) immunocompetent mice given intratumoral injection of splenic NK cells from CD45.2<sup>+</sup>*RII*<sup>WT</sup> mice or *RII*<sup>FL</sup> mice (**Fig. 4d–f**). We next assessed the proliferation of the transferred CD45.2<sup>+</sup> NK cells and converted intILC1s in the tumor microenvironment. Consistent with our transcriptomic analysis (**Fig. 3a–d**), we found more Ki67<sup>+</sup> intILC1s than Ki67<sup>+</sup> NK cells in CD45.1<sup>+</sup> mice (**Fig. 4g**). We also transferred NK cells from *RII*<sup>WT</sup> or

*RII*<sup>FL</sup> mice intratumorally into MCA1956-bearing CD45.1<sup>+</sup> host mice (**Fig. 4h**). The conversion of *RII*<sup>FL</sup> NK cells into intILC1s in the tumor microenvironment was significantly lower than that of *RII*<sup>WT</sup> NK cells (**Fig. 4i,j**). We sought to determine whether a correlation existed between the conversion of tumor NK cells and tumor progression. Therefore, we analyzed tumor group 1 ILC composition at various growth stages of MCA1956 tumors. Notably, over time and increasing tumor size, the proportion of tumor NK cells gradually decreased, while the fraction of intILC1s progressively increased (**Fig. 4k,l**). The frequency of tumor ILC1s remained steady at all stages of tumor progression (**Fig. 4k,l**). Overall, our results demonstrated a major role for TGF- $\beta$  signaling in regulating the cellular plasticity of group 1 ILCs in the tumor microenvironment.

### TGF- $\beta$ limits innate cancer immunosurveillance

To assess the function of TGF- $\beta$  signaling in group 1 ILCs and the conversion of NK cells into intILC1s and ILC1s, we assessed susceptibility to tumor initiation and growth in various cancer mouse

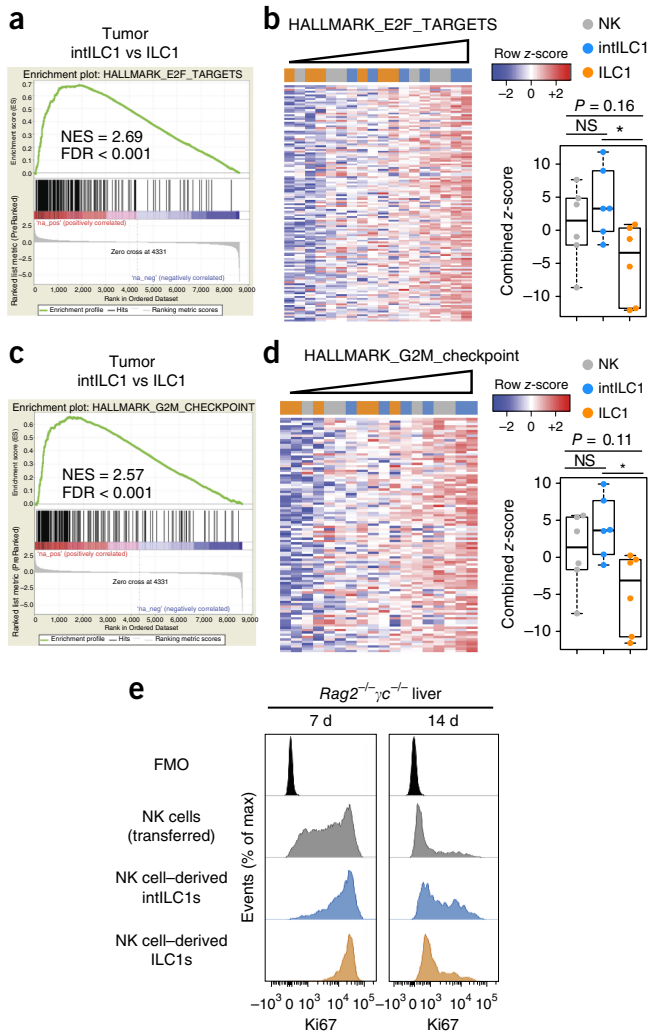


**Figure 3** intILC1s have the greatest proliferative capacity among group 1 ILC subsets *in vivo*. (a) GSEA of the set of genes that are targets of the transcription factor E2F (E2F\_TARGETS) in tumor intILC1s versus ILC1s. NES, normalized enrichment score. (b) Expression of the gene set in a, presented as row-wise z-scores of log<sub>2</sub>-transformed normalized RNA-sequencing read counts (left), and corresponding quantification by combined z-scores (right). (c) GSEA of the gene set encoding molecules in the G2-M checkpoint (G2M\_CHECKPOINT). (d) Expression of the gene set in c (left; presented as in b), and corresponding quantification by combined z-scores (right). NS, not significant ( $P > 0.05$ ); \* $P < 0.05$  (pairwise two-sided *t*-test with Benjamini and Hochberg (FDR) correction for multiple testing). (e) Flow cytometry of NK cell-derived group 1 ILC subsets in the liver of *Rag2*<sup>-/-</sup>*γC*<sup>-/-</sup> mice at 7 d ( $n = 3$  host mice) and 14 d ( $n = 4$  host mice) after the transfer of NK cells, assessing Ki67 expression. FMO (top), fluorescence minus one (control). Data are representative of one experiment with  $n = 6$  tumors (a–d; b, d (right): horizontal bars, median; boxes, 25th to 75th quartile; ‘whiskers’, 10th and 90th quartile) or one experiment (e).

models. The initiation of MCA-induced fibrosarcoma is controlled by NK cells, as suggested by the greater tumor penetrance in wild-type mice treated with depleting antibodies to the activating NK cell receptor NK1.1 (anti-NK1.1) or to the ganglioside asialo-GM1 (anti-asGM1) than in mice treated with control antibodies<sup>25,26</sup>. However, those experiments were performed before any description of ILC1s and thus did not address the role of these cells in immunosurveillance. Following the administration of a low dose of carcinogen

(25 μg MCA) to mice, we confirmed that treatment with anti-asGM1 significantly increased tumor initiation (Fig. 5a). The anti-apoptotic protein Mcl1 is induced by signaling via the common γ-chain receptor and is required for the maintenance of NK cells<sup>27</sup>. Through the use of mice with Cre recombinase-mediated deletion of loxP-flanked *Mcl1* alleles specifically in NKp46<sup>+</sup> cells (*Ncr1*<sup>cre/wt</sup>*Mcl1*<sup>fl/fl</sup>, called ‘*Mcl1*<sup>FL</sup>’ here), we found that Mcl1 was also required for the maintenance of NKp46<sup>+</sup> group 1 ILCs (Supplementary Fig. 4a,b). Using *Mcl1*<sup>FL</sup> mice and the appropriate control strains *Ncr1*<sup>cre/wt</sup>*Mcl1*<sup>fl/wt</sup> (called ‘*Mcl1*<sup>HET</sup>’ here) and *Ncr1*<sup>wt/wt</sup>*Mcl1*<sup>fl/fl</sup> (called ‘*Mcl1*<sup>WT</sup>’ here), we found support for the proposal of the critical importance of NKp46<sup>+</sup> cells in immunity to fibrosarcoma. *Mcl1*<sup>HET</sup> mice, which have a 50% lower abundance of all group 1 ILC subsets than that of *Mcl1*<sup>WT</sup> mice<sup>27</sup>, were more resistant to the development of fibrosarcoma than were *Mcl1*<sup>FL</sup> mice but were more sensitive to fibrosarcoma than were *Mcl1*<sup>WT</sup> mice (Fig. 5b). Interestingly, *Mcl1*<sup>FL</sup> mice (which are deficient in all group 1 ILC subsets) were as sensitive to fibrosarcoma formation as were wild-type mice treated with anti-asGM1 (Fig. 5a,b). Thus, we assessed the efficiency of anti-asGM1 in depleting wild-type mice of tumor group 1 ILCs. Anti-asGM1 depleted mice mainly of tumor NK cells and intILC1s and had only a minimal effect on tumor ILC1s (Supplementary Fig. 4c–h). Strikingly, *R1*<sup>CA-FL</sup> mice (which have tumor ILC1s and intILC1s but have a significantly lower frequency of NK cells than that of *R1*<sup>CA-WT</sup> mice) were as sensitive to the development of fibrosarcoma as were *Mcl1*<sup>FL</sup> mice and wild-type mice treated with anti-asGM1 (Fig. 5a,c), which suggested that the intILC1s and ILC1s in the tumors of *R1*<sup>CA-FL</sup> mice did not offer protection against tumor formation. A similar experiment using the same MCA dose additionally demonstrated greater resistance of *R1*<sup>FL</sup> mice than of *Ncr1*<sup>cre/wt</sup> mice to carcinogenesis (Fig. 5d). By using a higher dose of MCA (300 μg), we confirmed the greater resistance of *R1*<sup>FL</sup> mice than that of *Ncr1*<sup>cre/wt</sup> or *R1*<sup>WT</sup> mice (Fig. 5e).

Flow cytometry revealed a lower frequency of tumor NK cells and a higher frequency of ILC1s and intILC1s in MCA-induced fibrosarcomas from *R1*<sup>CA-FL</sup> mice than in those from *R1*<sup>CA-WT</sup> mice (Fig. 5f,g). In contrast, the frequency of tumor NK cells was significantly higher and the frequency of ILC1s and intILC1s was lower in fibrosarcomas from *R1*<sup>FL</sup> mice than in those from *R1*<sup>WT</sup> mice (Fig. 5f,g). *BRAF*<sup>V600E</sup> mutant SM1WT1 melanomas<sup>28</sup> were also infiltrated by tumor NK cells, intILC1s and ILC1s (Supplementary Fig. 5a). The growth of subcutaneously transplanted SM1WT1 tumors was significantly accelerated in *R1*<sup>CA-FL</sup> mice relative to their growth in *R1*<sup>CA-WT</sup> mice, and this was associated with more tumor intILC1s and ILC1s and fewer NK cells ( $P < 0.01$ ; Supplementary Fig. 5b,c). SM1WT1 melanomas grew significantly slower when transplanted into *R1*<sup>FL</sup> mice than when transplanted into *R1*<sup>WT</sup> mice ( $P < 0.001$ ; Supplementary Fig. 5d). In concert, SM1WT1 melanoma-bearing *R1*<sup>FL</sup> mice treated with anti-asGM1 showed accelerated tumor growth relative to that of SM1WT1 melanoma-bearing *R1*<sup>FL</sup> mice treated with control antibody (Supplementary Fig. 5d). Collectively, these data suggested that tumor NK cells were critical effector cells that restrained fibrosarcoma formation and melanoma growth. Moreover, our data suggested that ILC1s and intILC1s were incapable of performing this function. Thus, we identified TGF-β signaling in NKp46<sup>+</sup> cells as a suppressor of NK cell-mediated tumor immunosurveillance.

### NK cells control experimental metastasis

NK cells are reported to be critical for the control of tumor metastasis<sup>19,29</sup>. We therefore evaluated the role of TGF-β signaling in NKp46<sup>+</sup> cell-mediated control of B16F10 experimental lung metastasis. Mice with ablated TGF-β signaling in NKp46<sup>+</sup> cells (*R1*<sup>FL</sup> mice) showed

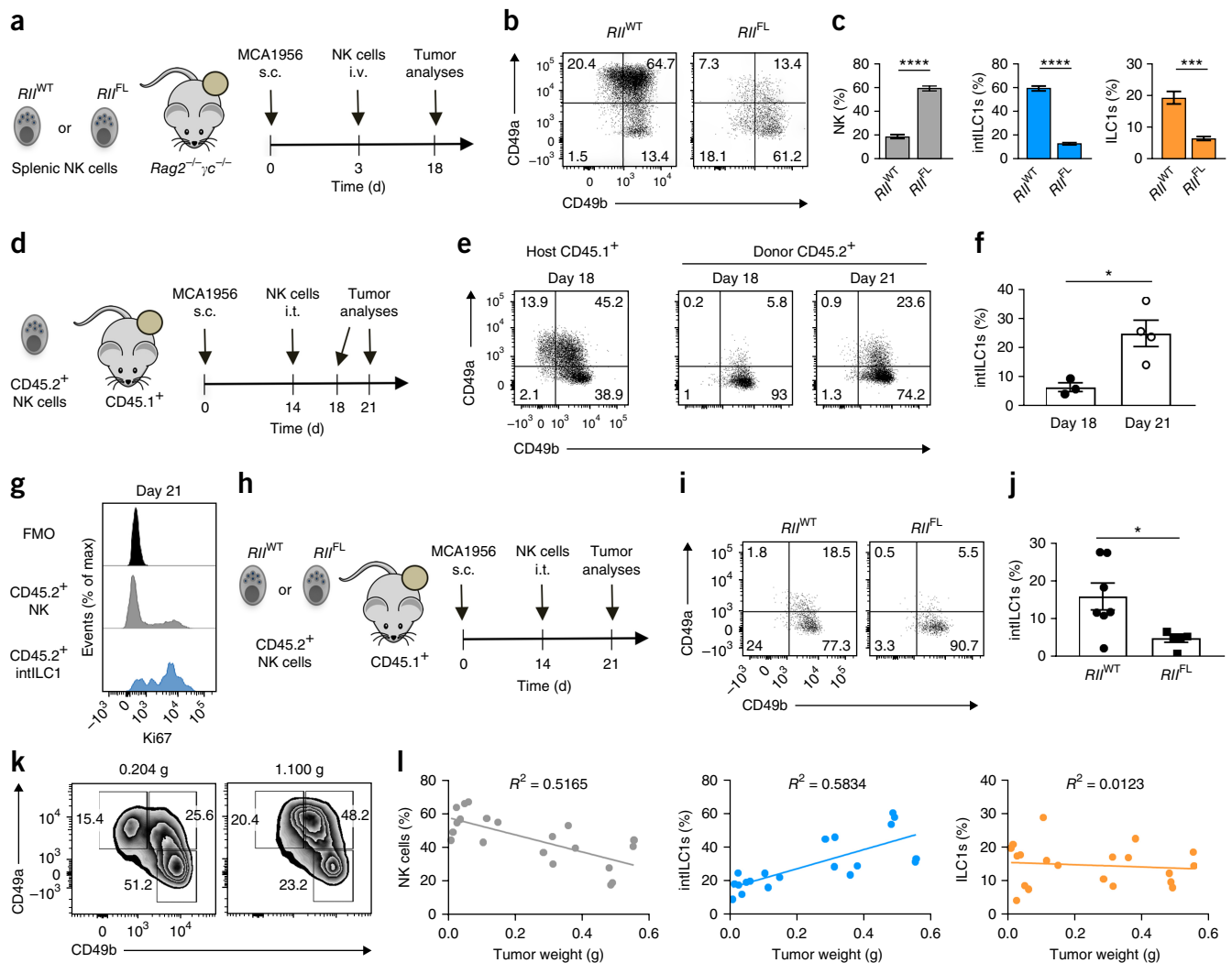


**Figure 4** TGF- $\beta$  induces the conversion of NK cells into intILC1s in the tumor microenvironment. **(a)** Experimental setup: *Rag2<sup>-/-</sup>γc<sup>-/-</sup>* mice were given subcutaneous (s.c.) transplantation of MCA1956 cells on day 0, followed by intravenous (i.v.) injection of  $5 \times 10^5$  splenic NK cells from *RII<sup>WT</sup>* or *RII<sup>FL</sup>* mice on day 3 and analysis on day 18 (time, below diagram). **(b)** Flow cytometry of *RII<sup>WT</sup>* or *RII<sup>FL</sup>* donor cells (above plots) from host mice as in **a** at day 18, showing tumor group 1 ILC subsets. **(c)** Quantification of tumor group 1 ILC subsets as in **b**. \*\*\*\* $P < 0.0001$  and \*\*\*\* $P < 0.0001$  (unpaired two-sided *t*-test). **(d)** Experimental setup: CD45.1<sup>+</sup> mice were given subcutaneous transplantation of MCA1956 cells on day 0, followed by intratumoral (i.t.) injection of CD45.2<sup>+</sup> splenic NK cells on day 14 and analysis on days 18 and 21. **(e)** Flow cytometry of host (CD45.1<sup>+</sup>) and donor (CD45.2<sup>+</sup>) tumor group 1 ILC subsets (above plots) from host mice as in **d** at day 18 or 21. **(f)** Quantification of NK cell-derived intILC1s as in **e**. \* $P < 0.05$  (unpaired two-sided *t*-test). **(g)** Flow cytometry of donor (CD45.2<sup>+</sup>) NK cells and intILC1s (left margin) isolated from MCA1956 tumors in mice as in **d**, assessing Ki67 expression. **(h)** Experimental setup: CD45.1<sup>+</sup> mice were given subcutaneous transplantation of MCA1956 cells on day 0, followed by intratumoral injection of CD45.2<sup>+</sup>*RII<sup>WT</sup>* or *RII<sup>FL</sup>* splenic NK cells on day 14 and analysis on day 21. **(i)** Flow cytometry of *RII<sup>WT</sup>* or *RII<sup>FL</sup>* donor cells (above plots) from host mice as in **h**, showing tumor group 1 ILC subsets. **(j)** Quantification of NK cell-derived intILC1s as in **i**. \* $P < 0.05$  (unpaired two-sided *t*-test). **(k)** Flow cytometry of cells from a small MCA1956 tumor (0.204 g) and a large MCA1956 tumor (1.100 g), showing tumor group 1 ILC subsets. **(l)** Correlation of the frequency of NK cells (left), intILC1s (middle) or ILC1s (right) and tumor weight (linear regression analysis;  $P = 0.0004$  (NK cells),  $P < 0.001$  (intILC1s) and  $P = 0.6416$  (ILC1s)). Each symbol (**f**, **j**, **l**) represents an individual mouse; small horizontal lines (**f**, **j**) indicate the mean ( $\pm$  s.e.m.). Data are representative of one experiment with  $n = 6$  host mice (**b**, **c**; mean  $\pm$  s.e.m. in **c**), one experiment with  $n = 3$  (day 18) or  $n = 4$  (day 21) host mice (**e**–**g**) or one experiment with  $n = 7$  host mice given *RII<sup>WT</sup>* cells or  $n = 5$  hosts given *RII<sup>FL</sup>* cells (**i**, **j**) or are pooled from five different experiments with  $n = 20$  mice (**k**, **l**).

significantly fewer B16F10 lung metastasis than that of wild-type, *RII<sup>WT</sup>* or *Ncr1<sup>cre/wt</sup>* mice (**Fig. 6a**). Mice with constitutively active TGF- $\beta$  signaling in NKp46<sup>+</sup> cells (*RI<sup>CA-FL</sup>* mice) displayed a significantly greater burden of B16F10 lung metastases than that of *RI<sup>CA-WT</sup>*, wild-type, *RII<sup>WT</sup>* or *Ncr1<sup>cre/wt</sup>* mice (**Fig. 6a**). These results could be explained in part by the lack of NK cells in *RI<sup>CA-FL</sup>* mice. Moreover, our data suggested that ILC1s and intILC1s in *RI<sup>CA-FL</sup>* mice were also unable to restrict lung metastasis. To confirm that, we injected

a lower number of B16F10 melanoma cells than used above (**Fig. 6a**) into *RI<sup>CA-FL</sup>*, *Mcl1<sup>FL</sup>* or wild-type mice treated with anti-asGM1. Most strikingly, untreated *RI<sup>CA-FL</sup>* mice were more sensitive to experimental metastasis than were untreated *Mcl1<sup>FL</sup>* mice or wild-type mice treated with anti-asGM1 (**Fig. 6b**). These results indicated that TGF- $\beta$ -induced intILC1s and ILC1s might even promote metastasis. That hypothesis was supported by the finding that treatment with anti-asGM1 reduced the number of B16F10 metastasis in *RI<sup>CA-FL</sup>* mice

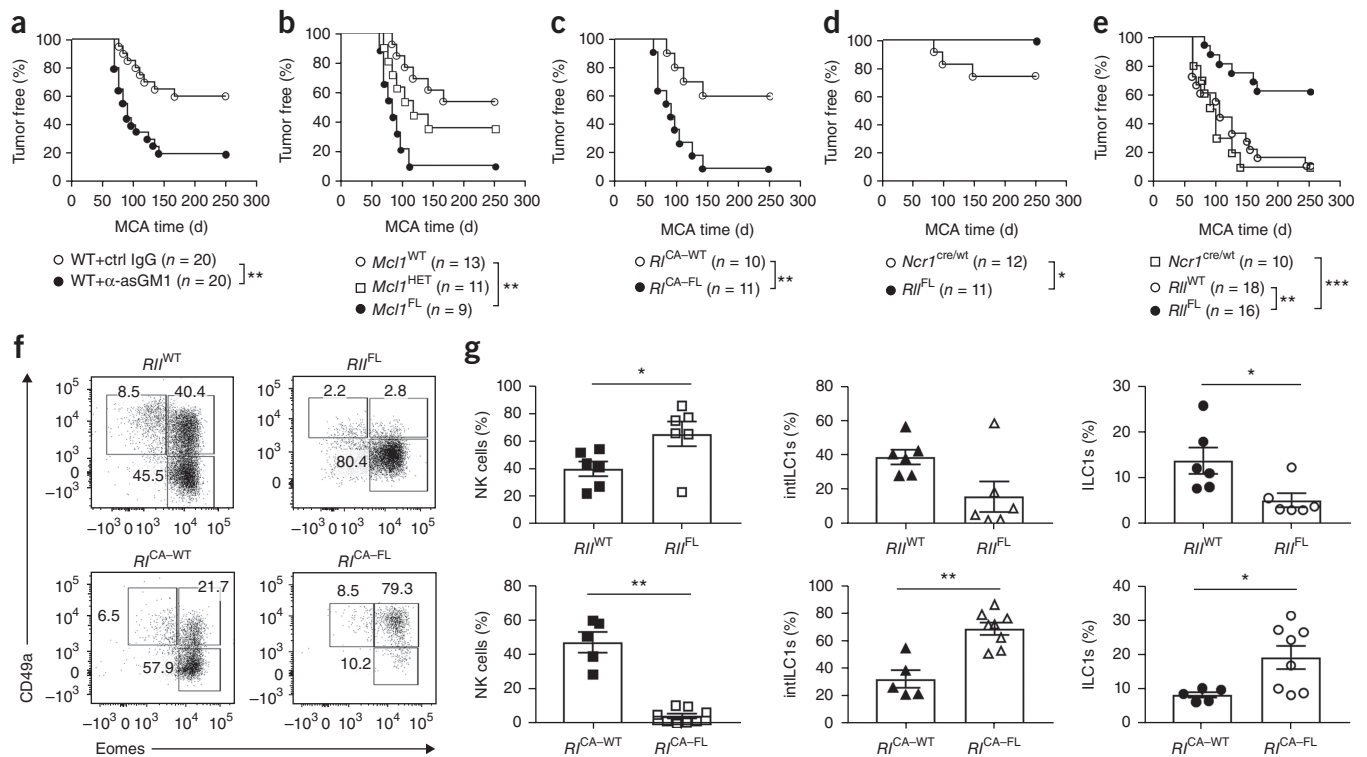


**Figure 5** TGF- $\beta$  signaling limits tumor immunosurveillance by converting tumor NK cells into intILC1s and ILC1s. (**a–e**) Tumor incidence of C57BL/6 wild-type (WT) mice treated with anti-asGM1 ( $\alpha$ -asGM1) or immunoglobulin G, as a control (ctrl IgG) (**a**), or of *Mcl1*<sup>WT</sup>, *Mcl1*<sup>HET</sup> and *Mcl1*<sup>FL</sup> mice (**b**), *R1*<sup>CA-WT</sup> and *R1*<sup>CA-FL</sup> mice (**c**), *Ncr1*<sup>cre/wt</sup> and *R1*<sup>FL</sup> mice (**d**) or *Ncr1*<sup>cre/wt</sup>, *R1*<sup>WT</sup> and *R1*<sup>FL</sup> mice (**e**), over time (horizontal axes) after subcutaneous injection of 25  $\mu$ g MCA (**a–d**) or 300  $\mu$ g MCA (**e**). \* $P$  < 0.05, \*\* $P$  < 0.01 and \*\*\* $P$  < 0.001 (log-rank test). (**f**) Flow cytometry of cells from MCA-induced fibrosarcomas of *R1*<sup>WT</sup>, *R1*<sup>FL</sup>, *R1*<sup>CA-WT</sup> and *R1*<sup>CA-FL</sup> mice (above plots), showing tumor group 1 ILC composition. (**g**) Quantification of tumor NK cells (left), intILC1s (middle) ILC1s (right) from *R1*<sup>WT</sup> mice ( $n$  = 6) and *R1*<sup>FL</sup> mice ( $n$  = 6) (top row) or *R1*<sup>CA-WT</sup> mice ( $n$  = 5) and *R1*<sup>CA-FL</sup> mice ( $n$  = 8) (bottom row). \* $P$  < 0.05 and \*\* $P$  < 0.01 (Mann-Whitney  $U$ -test). Each symbol (**g**) represents an individual mouse. Data are representative of one experiment (**a–c, f, g**; mean  $\pm$  s.e.m. in **g**) or two experiments (**d, e**).

to a level similar to that in *R1*<sup>CA-WT</sup> mice treated with anti-asGM1 (Fig. 6c). RM-1 is an aggressive prostate cancer cell line, and RM-1 lung metastases were fewer in *R1*<sup>FL</sup> mice and greater in *R1*<sup>CA-FL</sup> mice than in their corresponding control strains (Supplementary Fig. 6a). Notably, we confirmed, in the RM-1 model, our results showing that treatment with anti-asGM1 reduced the number of lung metastasis in *R1*<sup>CA-FL</sup> mice (Fig. 6d). Of note, the administration of anti-asGM1 did not affect the number of lung metastasis in *Mcl1*<sup>FL</sup> mice (Fig. 6e). After intravenous injection of the mCherry<sup>+</sup> breast cancer cell line E0771-LMB, the number of lung metastases of these cells was also greater in *R1*<sup>CA-FL</sup> mice than in *Ncr1*<sup>cre/wt</sup> mice (Supplementary Fig. 6b–d). Notably, TGF- $\beta$  signaling in NKp46<sup>+</sup> cells appeared to be less important in this tumor model, since *R1*<sup>FL</sup> mice were no more resistant to metastasis than were *Ncr1*<sup>cre/wt</sup> control mice (Supplementary Fig. 6b–d). Overall, these data supported the proposal that NK cells were the main population that restrained tumor metastasis, while ILC1-like cells (tumor intILC1s and ILC1s) under constitutively active TGF- $\beta$  signaling (in *R1*<sup>CA-FL</sup> mice) were unable to control, and possibly promoted, metastasis. Together our data raised the question of how the intILC1s and ILC1s limited innate immunosurveillance.

### Distinct functions of tumor ILC1s

We next assessed functional differences among tumor group 1 ILC subsets. Notably, the expression of genes encoding inhibitory immunological checkpoint receptors, such as CTLA-4, CD96 and LAG-3, was

higher in tumor ILC1s and intILC1s than in tumor NK cells (Fig. 7a). Those differences were further confirmed at the protein level by flow cytometry (Fig. 7b and Supplementary Fig. 7a,b). Tumor ILC1s also showed higher expression of genes encoding the inhibitory NK cell receptors NKG2A and KLRG1 than that of tumor NK cells (Fig. 7a and Supplementary Fig. 7c). One of the gene sets most upregulated in tumor ILC1s relative to its expression in NK cells, as determined by GSEA, encoded products related to angiogenesis (Fig. 7c). Indeed, we detected a higher concentration of the pro-angiogenic molecule PDGF-AB in supernatants from tumor ILC1s activated with the phorbol ester PMA and ionomycin than in their intILC1 or NK cell counterparts (Fig. 7d). Moreover, stimulation of the mouse endothelial cell line bEND.5 with supernatants of tumor intILC1s and ILC1s induced more endothelial tubes than did stimulation of that cell line with supernatants of tumor NK cells (Fig. 7e). Tumor ILC1s also showed more production and secretion of the myeloid growth factor GM-CSF than that of tumor NK cells, while tumor NK cells were superior producers of the T cell and NK cell chemoattractant RANTES (Fig. 7f,g). These results indicated that various pathways known to be involved in tumor progression, metastasis and therapy resistance were upregulated in tumor intILC1s and ILC1s relative to their activity in NK cells.

### TNF promotes resistance to innate immunosurveillance

We were intrigued by the finding that tumor NK cells had higher expression of interferon- $\gamma$  (IFN- $\gamma$ ) and lower expression of TNF than that of intILC1s or ILC1s (Fig. 8a). After stimulation with PMA and

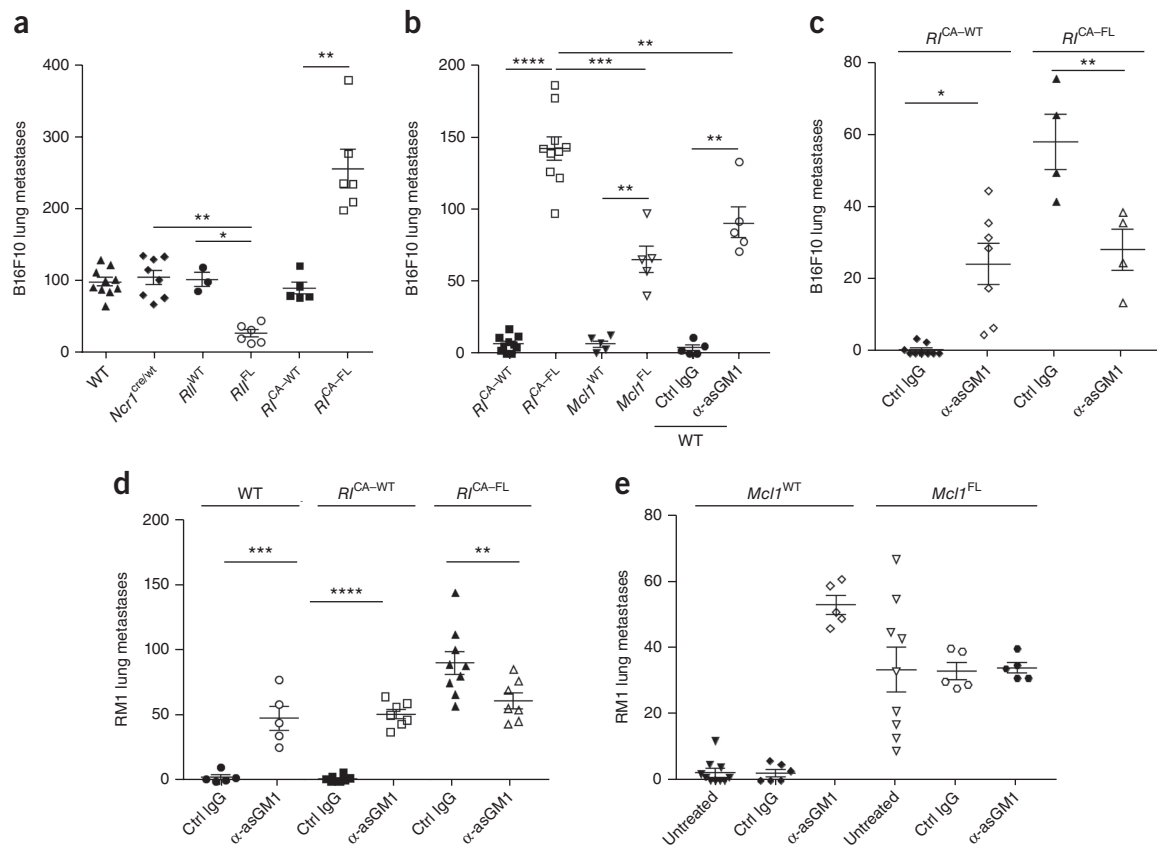


**Figure 6** TGF- $\beta$  signaling abolishes control of metastasis by the innate immune system. Quantification of experimental lung metastases in wild-type, *Ncr1<sup>cre/wt</sup>*, *R11<sup>WT</sup>*, *R11<sup>FL</sup>*, *R1<sup>CA-WT</sup>* and *R1<sup>CA-FL</sup>* mice 14 d after intravenous injection of  $1 \times 10^5$  B16F10 melanoma cells (a); in *R1<sup>CA-WT</sup>*, *R1<sup>CA-FL</sup>*, *Mcl1<sup>WT</sup>*, *Mcl1<sup>FL</sup>* and wild-type mice 14 d after intravenous injection of  $1 \times 10^4$  B16F10 melanoma cells, with wild-type mice treated with anti-asGM1 or the control antibody IgG (horizontal axis) (b); in *R1<sup>CA-WT</sup>* or *R1<sup>CA-FL</sup>* mice 14 d after intravenous injection of  $5 \times 10^3$  B16F10 melanoma cells, in mice treated with anti-asGM1 or IgG (horizontal axis) (c); in wild-type, *R1<sup>CA-WT</sup>* or *R1<sup>CA-FL</sup>* mice 14 d after intravenous injection of  $1 \times 10^4$  RM-1 prostate cancer cells, in mice treated with anti-asGM1 or IgG (horizontal axis) (d); or in *Mcl1<sup>WT</sup>* or *Mcl1<sup>FL</sup>* mice 14 d after intravenous injection of  $1 \times 10^4$  RM-1 prostate cancer cells, with or without (untreated) treatment with anti-asGM1 or IgG (horizontal axis) (e). Each symbol represents an individual mouse; small horizontal lines indicate the mean ( $\pm$  s.e.m.). \* $P < 0.05$ , \*\* $P < 0.01$ , \*\*\* $P < 0.001$  and \*\*\*\* $P < 0.0001$  (one-way analysis of variance (ANOVA) and Tukey's multiple-comparisons test). Data are from one experiment with  $n = 10$  wild-type mice,  $n = 10$  *Ncr1<sup>cre/wt</sup>* mice,  $n = 3$  *R11<sup>WT</sup>* mice,  $n = 6$  *R11<sup>FL</sup>* mice,  $n = 5$  *R1<sup>CA-WT</sup>* mice and  $n = 6$  *R1<sup>CA-FL</sup>* mice (a), one experiment with  $n = 10$  *R1<sup>CA-WT</sup>* mice,  $n = 10$  *R1<sup>CA-FL</sup>* mice,  $n = 5$  *Mcl1<sup>WT</sup>* mice,  $n = 5$  *Mcl1<sup>FL</sup>* mice or  $n = 5$  wild-type mice per group (b), one experiment with  $n = 7$  *R1<sup>CA-WT</sup>* mice per group or  $n = 4$  *R1<sup>CA-FL</sup>* mice per group (c), two pooled experiments with  $n = 5$  wild-type mice per group,  $n = 8$  *R1<sup>CA-WT</sup>* mice (ctrl IgG),  $n = 7$  *R1<sup>CA-WT</sup>* mice (anti-asGM1),  $n = 9$  *R1<sup>CA-FL</sup>* mice (ctrl IgG) or  $n = 7$  *R1<sup>CA-FL</sup>* mice (anti-asGM1) (d) or two pooled experiments with  $n = 10$  *Mcl1<sup>WT</sup>* mice (untreated),  $n = 6$  *Mcl1<sup>WT</sup>* mice (ctrl IgG),  $n = 5$  *Mcl1<sup>WT</sup>* mice (anti-asGM1),  $n = 9$  *Mcl1<sup>FL</sup>* mice (untreated),  $n = 5$  *Mcl1<sup>FL</sup>* mice (ctrl IgG) or  $n = 5$  *Mcl1<sup>FL</sup>* mice (anti-asGM1) (e).

ionomycin, all tumor group 1 ILC subsets had a similar frequency of IFN- $\gamma^+$  cells, while ILC1 and intILC1 populations had significantly more TNF-producing cells than did tumor NK cell populations (Fig. 8a,b). Thus, tumor NK cell populations had a higher ratio of IFN- $\gamma^+$  cells to TNF $^+$  cells than that of ILC1 or intILC1 populations (Fig. 8b), which coincided with their beneficial role in tumor control. Similar cytokine profiles were observed for tumor group 1 ILCs isolated from SM1WT1 melanomas (Supplementary Fig. 8a). To assess the function of IFN- $\gamma$  and TNF in the growth and metastasis of tumors, we conducted cytokine-neutralization studies (Fig. 8c and Supplementary Fig. 8b). Using two different tumor models (MCA1956 and SM1WT1), we demonstrated that IFN- $\gamma$  was important in limiting tumor growth, whereas TNF probably fueled tumor growth, in *R11<sup>WT</sup>* mice (Fig. 8d and Supplementary Fig. 8c). Strikingly, neutralization of TNF in *R11<sup>FL</sup>* mice limited tumor growth to a lesser extent, in line with the reduction in the number of tumor intILC1s and ILC1s via ablation of TGF- $\beta$  signaling in the NKp46 $^+$  cell populations (Fig. 8d and

Supplementary Fig. 8c). In the next set of experiments, we assessed the role of IFN- $\gamma$  and TNF in experimental metastasis using B16F10 and RM1 cell lines (Fig. 8e). Antibody-mediated neutralization of IFN- $\gamma$  increased the number of metastasis in the lungs of wild-type and *R11<sup>FL</sup>* mice, whereas similarly treated *R1<sup>CA-FL</sup>* mice only showed a slight increase in the number of metastasis (Fig. 8f,g). On the other hand, neutralization of TNF reduced the number of lung metastasis in wild-type and *R1<sup>CA-FL</sup>* mice, whereas similarly treated *R11<sup>FL</sup>* mice only showed a slight decrease in metastasis (Fig. 8f,g). Even though TNF expressed by innate cells might be one mechanism for limiting immunosurveillance, the intILC1s and ILC1s probably generated a pro-tumorigenic microenvironment by a variety of pathways (for example, immunomodulation and angiogenesis).

#### Human tumor ILC1-like cells

NK cell-derived IFN- $\gamma$  can be used to predict the survival of patients with gastrointestinal stromal tumors (GISTs) undergoing targeted therapy

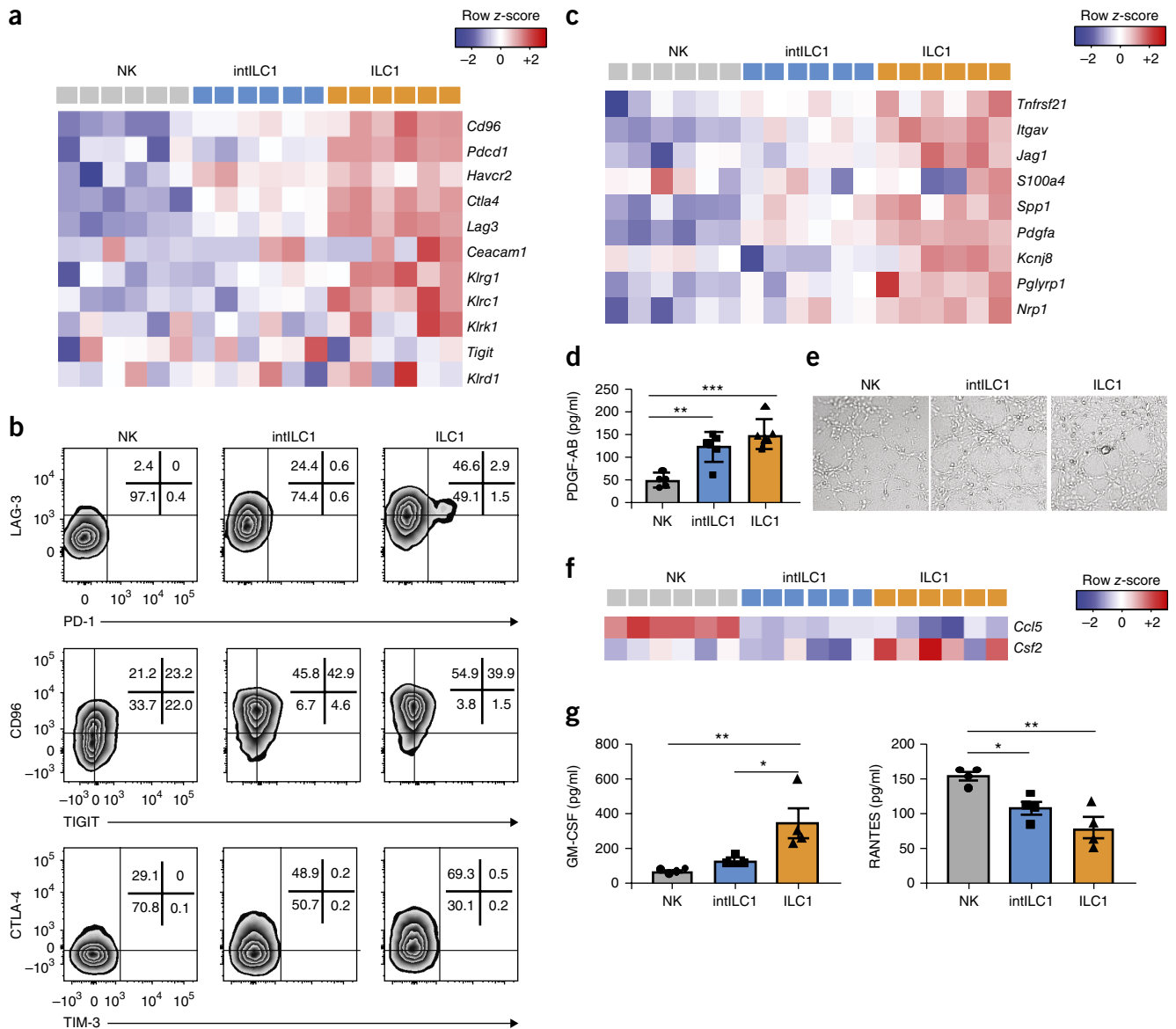


**Figure 7** Functional differences among tumor group 1 ILC subsets. **(a)** Expression of genes encoding immunological receptors (right margin) in tumor NK cells, intILC1s and ILC1s (change in expression of over 1-fold ( $\log_2$  values) and  $FDR < 0.01$ ). Select genes and products: *Klrc1*, *NKG2A*; *Klrg1*, KLRG1. **(b)** Flow cytometry of tumor NK cells, intILC1s and ILC1s (above plots), assessing expression of immunological checkpoint receptors. **(c)** Expression of genes encoding angiogenesis-related molecules (right margin) in tumor NK cells, intILC1s and ILC1s (presented as in **a**). **(d)** ELISA of PDGF-AB in supernatants of tumor NK cells, intILC1s and ILC1s (horizontal axis) stimulated with PMA and ionomycin. \*\*  $P < 0.01$  and \*\*\*  $P < 0.001$  (one-way ANOVA and Tukey's multiple-comparisons test). **(e)** Tube formation by bEND.5 endothelial cells 4 h after stimulation with supernatants of tumor NK cells, intILC1s or ILC1s (above images) stimulated with PMA and ionomycin. Original magnification,  $\times 20$ . **(f)** Expression of *Csf2* (encoding GM-CSF) and *Ccl5* (encoding RANTES) by tumor NK cells, intILC1s and ILC1s (above plots). **(g)** Multiplex-bead-based analysis of GM-CSF and RANTES in supernatants of tumor NK cells, intILC1s and ILC1s (horizontal axes) stimulated with PMA and ionomycin. \*  $P < 0.05$  and \*\*  $P < 0.01$  (one-way ANOVA and Tukey's multiple-comparisons test). Each symbol (**d,g**) represents an individual sample. Data are representative of one experiment (**a,c,f**) or two independent experiments with  $n = 7$  tumors (**b**) or  $n = 5$  tumors (**e**) or are from two independent experiments with  $n = 5$  mice (NK cells) or  $n = 6$  mice (intILC1 and ILC1s) (**d**; mean  $\pm$  s.e.m.) or one experiment with  $n = 4$  tumors (**g**; mean  $\pm$  s.e.m.).

with imatinib mesylate (the mesylate salt of the tyrosine-kinase inhibitor imatinib)<sup>30</sup>. Since it is clear that NK cells are important for the control of GISTs<sup>31</sup>, we used the chemokine receptor CXCR6, a well-established marker of human and mouse ILC1s<sup>32</sup>, to identify human ILC1-like cells among peripheral blood mononuclear cells (PBMCs) and tumor-infiltrating lymphocytes (TILs) from patients with GISTs. We detected a significantly greater proportion of viable Lin<sup>-</sup> (CD19<sup>-</sup>CD14<sup>-</sup>CD3<sup>-</sup>)

CD56<sup>+</sup>CXCR6<sup>+</sup> ILC1-like cells among the TILs than among the PBMCs of patients with GISTs ( $P < 0.05$ ; **Fig. 8h** and **Supplementary Fig. 8d**). Notably, CXCR6 was also selectively expressed on tumor ILC1s isolated from MCA1956 tumors (**Figs. 1e** and **8i** and **Supplementary Fig. 8e**). Thus, further studies are needed to delineate how ILC1s can affect the tumor microenvironment and limit NK cell-mediated immunosurveillance in mice and humans.

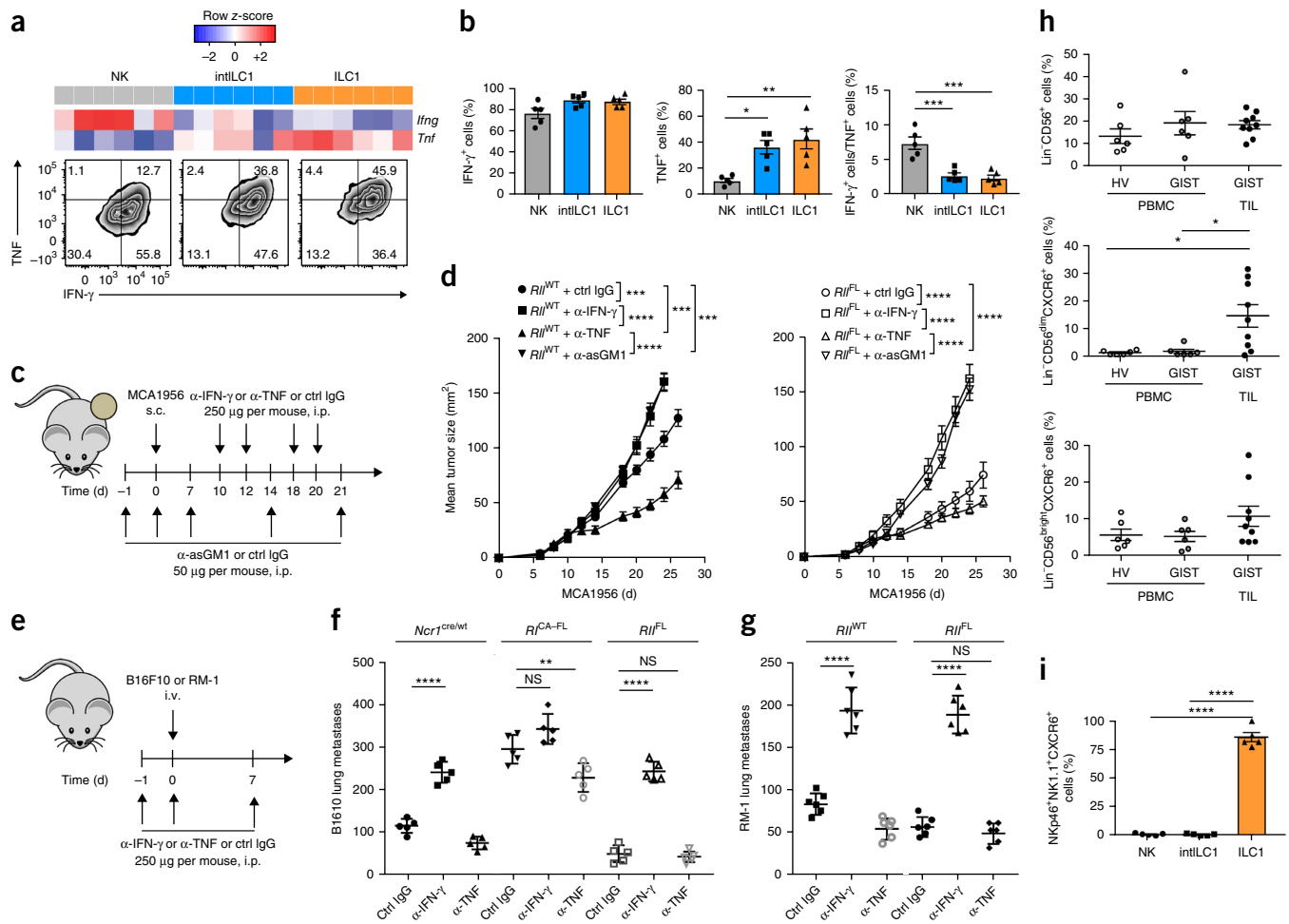


**Figure 8** IFN- $\gamma$  and TNF control tumor growth and metastasis differentially. **(a)** Expression of genes encoding IFN- $\gamma$  (*Ifng*) and TNF (*Tnf*) (top), and flow cytometry analyzing the expression of IFN- $\gamma$  and TNF (bottom), in tumor NK cells, intILC1s and ILC1s (above plots). **(b)** Quantification of IFN- $\gamma$ -producing (left) and TNF-producing (middle) NK cells, intILC1s and ILC1s obtained from MCA1956 tumors and stimulated with PMA and ionomycin, assessed by flow cytometry, and the ratio of IFN- $\gamma$ -producing cells to TNF-producing cells (IFN- $\gamma$ <sup>+</sup> cells/TNF<sup>+</sup> cells; right). \* $P < 0.05$ , \*\* $P < 0.01$  and \*\*\* $P < 0.001$  (one-way ANOVA and Tukey's multiple-comparisons test). **(c)** Experimental setup: mice were given intraperitoneal (i.p.) injection of anti-asGM1 or IgG (below diagram) before and after subcutaneous transplantation of MCA1956 cells on day 0, along with intraperitoneal injection of anti-IFN- $\gamma$ , anti-TNF or IgG (control antibody) after cell transplantation (above diagram). **(d)** Tumor growth in *RII*<sup>WT</sup> mice (left) and *RII*<sup>FL</sup> mice (right) treated as in **(c)** (key), assessed over time after transplantation of MCA1956 cells (horizontal axis). \*\*\* $P < 0.001$  and \*\*\*\* $P < 0.0001$  (one-way ANOVA and Tukey's multiple-comparisons test at endpoint). **(e)** Experimental setup for antibody-mediated cytokine neutralization in experimental metastasis: mice were given intraperitoneal injection of anti-IFN- $\gamma$ , anti-TNF or IgG (control antibody) before and after intravenous injection of B16F10 or RM-1 cells on day 0. **(f,g)** Quantification of lung metastases in *Ncr1*<sup>cre/wt</sup>, *RJA-FL*, *RII*<sup>FL</sup> and *RII*<sup>WT</sup> mice (above plots) challenged intravenously with  $1 \times 10^5$  B16F10 cells (**f**) or  $1 \times 10^4$  RM-1 cells (**g**) and treated with antibodies as in **(e)** (horizontal axes). \*\* $P < 0.01$ , \*\*\*\* $P < 0.0001$  (one-way ANOVA and Tukey's multiple comparison test). **(h)** Frequency of Lin-CD56<sup>dim</sup> CXCR6<sup>+</sup> cells (left), CXCR6<sup>+</sup> cells among Lin-CD56<sup>dim</sup> cells (middle) and CXCR6<sup>+</sup> cells among Lin-CD56<sup>bright</sup> cells (right) in PBMC and TIL populations (below plots) from healthy volunteers (HV) and patients with GISTs (horizontal axes), assessed by flow cytometry. \* $P < 0.05$  (one-way ANOVA and Tukey's multiple-comparisons test). **(i)** Frequency of NK cells, intILC1s and ILC1s among CXCR6<sup>+</sup> group 1 ILCs from MCA1956 tumors, assessed by flow cytometry. \*\*\*\* $P < 0.0001$  (one-way ANOVA and Tukey's multiple-comparisons test). Each symbol (**b,f,g,h,i**) represents an individual mouse (**b,f,g,i**) or donor (**h**); small horizontal lines (**f,g,h**) indicate the mean ( $\pm$  s.e.m.). Data are representative of one experiment (**a**), are from one experiment with  $n = 5$  mice per group (**b**; mean  $\pm$  s.e.m.) or two experiments with  $n = 5$  mice per group (**d**; mean  $\pm$  s.e.m.) or  $n = 5$  (**f**) or  $n = 6$  (**g**) mice per group (**f,g**), are representative of one experiments with  $n = 6$  donors per group (PBMCs) or  $n = 9$  donors (TILs) (**h**) or are from two independent experiments with  $n = 5$  mice (**i**; mean  $\pm$  s.e.m.).

## DISCUSSION

In our study we found that TGF- $\beta$  signaling in NKp46<sup>+</sup> cells drove the conversion of NK cells (CD49a<sup>-</sup>CD49b<sup>+</sup>) into intILC1s (CD49a<sup>+</sup>CD49b<sup>+</sup>) and ILC1s (CD49a<sup>+</sup>CD49b<sup>-</sup>) in the tumor micro-environment. Moreover, this conversion was also observed when we reconstituted lymphocyte-deficient *Rag2*<sup>-/-</sup>*γc*<sup>-/-</sup> mice with splenic NK cells. Our findings in different primary and transplantable tumor models support the proposal of a critical protective role for NK cells,

while intILC1s and ILC1s were unable to restrain tumor growth and metastasis. This might be explained, at least in part, by the finding of a lower ratio of IFN- $\gamma$  production to TNF production and increased expression of immunological checkpoint receptors as tumors grew and the finding that the proportion of tumor-associated NK cells decreased with their conversion into intILC1s and ILC1s. Overall, our data strengthen the novel concept that tumor group 1 ILC subsets are highly plastic and convert in a context-dependent manner. This

defines a previously unknown mechanism whereby TGF- $\beta$  signaling drives evasion of the immune system by converting NK cells into intILC1s and ILC1s in the tumor microenvironment.

Most previous observations concerning tumor-infiltrating NK cells were made before the concept of ILC1s. Limited data suggest that ILC1-like cells can either promote tumorigenesis or foster anti-tumor immune responses, depending on the tissue context and ILC1 phenotype<sup>33,34</sup>. Here, flow cytometry and global transcriptomic analysis showed that tumor NK cells (CD49a<sup>+</sup>CD49b<sup>+</sup>) and ILC1s (CD49a<sup>+</sup>CD49b<sup>-</sup>) were accompanied by an intermediate CD49a<sup>+</sup>CD49b<sup>+</sup> (intILC1) subset that shared phenotypic characteristics with both tumor NK cells and ILC1s. Interestingly, as tumors grew, the proportion of tumor NK cells diminished, while the proportion of intILC1s increased. That observation was in line with enhanced proliferative capacity of intILC1s.

It has been suggested that subsequent to their divergent lineage specification, NK cells and ILC1s possess developmental plasticity<sup>35</sup>, and TGF- $\beta$  signaling in Ncr1<sup>+</sup> (Nkp46<sup>+</sup>) cells has been shown to be important for maintaining the phenotype of CD49a<sup>+</sup> salivary gland ILC1s, a population distinct from NK cells in this organ<sup>20</sup>. Those studies lacked any description of the consequences of NK cell plasticity on the immune response, in particular on tumor control. Specifically, our work is the first, to our knowledge, to describe and characterize this TGF- $\beta$ -driven CD49a<sup>+</sup>CD49b<sup>+</sup> intILC1 population in tumors that shared features of both NK cells and ILC1s but also had unique features and a positive correlation with tumor progression. Interestingly, the conversion of NK cells into intILC1 was also seen after the transfer of wild-type splenic NK cells into lymphocyte-deficient mice, as well as for NK cells cultured *in vitro* in TGF- $\beta$ . The conversion of NK cells in tumors was dependent on time and TGF- $\beta$ . Unexpectedly, we did not find evidence for increased canonical TGF- $\beta$  signaling among tumor group 1 ILC subsets in our transcriptomic analyses. This suggests that non-canonical TGF- $\beta$  signaling might be involved in the conversion of NK cells and is in line with the finding that loss of the transcription factor SMAD4 in Nkp46<sup>+</sup> cells promotes a non-canonical TGF- $\beta$ -driven conversion of NK cells into ILC1-like cells<sup>36</sup>. Collectively, these data highlight the importance of TGF- $\beta$  in the conversion of NK cells; however, they also suggest that other pathways can influence the balance among group 1 ILC subsets under steady-state and pathophysiological conditions.

Our results raise questions about the functional differences among group 1 ILC subsets and their role in tumor pathogenesis. We conclusively described a host-protective effector function of NK cells (rather than ILC1s) in mouse models of tumor initiation, growth and metastasis. It has been reported that tissue-resident ILCs and innate-like T cells control tumor surveillance<sup>34</sup>. Those conclusions were based on the assumption that all NK cells are dependent on the transcription factor Nfil3, and they relied on the use of mice deficient in the cytokine IL-15. However, not all NK cells are Nfil3 dependent<sup>13</sup>, and IL-15-deficient and Nfil3-deficient mice have additional defects that might explain why these strains do not behave like each other. In contrast, a published study has demonstrated that a unique ILC population isolated from TILs from high-grade serous tumors inhibits the proliferation and activation of T cells<sup>33</sup>. In our experiments, a reduction in the abundance of tumor NK cells, even in the presence of intILC1s and ILC1s, caused mice to be critically compromised in their control of carcinogen-induced tumor formation and tumor metastasis. Notably, *R1CA-FL* mice displayed greater tumor metastasis than that of mice lacking all NK cells and ILC1s (*Mcl1<sup>FL</sup>* mice). Depletion using anti-asGM1 reduced experimental tumor metastasis in *R1CA-FL* mice in two different models. In line with our findings, CD49a<sup>+</sup>CD49b<sup>+</sup> cells have been shown to fail to control B16F10

lung metastasis or to contain infection with mouse cytomegalovirus<sup>36</sup>. This suggests that under TGF- $\beta$  signaling, intILC1s and ILC1s offer no protection from tumor formation and might even promote metastasis.

Interestingly, tumor NK cell populations showed a higher ratio of IFN- $\gamma$ <sup>+</sup> cells to TNF<sup>+</sup> cells than that of intILC1 or ILC1 populations. Given that IFN- $\gamma$  is anti-angiogenic<sup>37</sup> and is considered a critical host factor for tumor immunosurveillance<sup>38</sup> and that TNF has pro-tumorigenic and pro-angiogenic properties<sup>39–41</sup>, the ratio of IFN- $\gamma$ <sup>+</sup> cells to TNF<sup>+</sup> cells suggested that tumor NK cells had stronger anti-tumor properties than those of intILC1s or ILC1s. Furthermore, we demonstrated in the cytokine-depletion experiments that IFN- $\gamma$  was host protective, while TNF was tumor promoting. It remains to be elucidated, through the use of mice with conditional gene targeting, how important the production of TNF by Nkp46<sup>+</sup> cells is for the control of tumors, given that other tumor populations, notably myeloid cells, also make substantial amounts of TNF. The upregulated expression of immunological checkpoint molecules in tumor intILC1s and ILC1s, relative to their expression in NK cells, also suggested that intILC1s and ILC1s might be functionally impaired. Additionally, loss of Eomes expression in tumor-infiltrating NK cells is a reported hallmark of NK cell exhaustion<sup>42</sup>, and perhaps the transition of NK cells to ILC1s explains this observation in part.

The composition of group 1 ILCs in end-stage mouse tumors, as we described, was very similar to what has been observed for decidual NK cells (dNK cells)<sup>43</sup>. In humans, a phenotypic similarity between tumor-infiltrating NK cells and dNK cells has also been reported<sup>44</sup>. Those tumor-infiltrating NK cells possessed angiogenic ability, which probably resulted from TGF- $\beta$  exposure<sup>45</sup>. dNK cells drive angiogenesis in early pregnancy<sup>46</sup>, and dNK cells induce indoleamine 2,3-dioxygenase in decidual myelomonocytic CD14<sup>+</sup> cells and promote the generation of regulatory T cells<sup>47</sup>, which contributes to maternal–fetal tolerance. Further work is now needed in mice and humans to establish what functions intILC1s and ILC1s have in tumor angiogenesis and pathogenesis and the crosstalk of those cells with other cell populations in the tumor microenvironment.

Anti-TGF- $\beta$  therapies have long been proposed and tested in mice<sup>48,49</sup> and humans<sup>50</sup> with various possible indications, including cancer<sup>51</sup>. Those therapies were designed on the basis of the very pleiotropic immunosuppressive effects of TGF- $\beta$ , and it is unclear at this stage whether neutralizing TGF- $\beta$  would be an effective approach in cancer. Our findings support the proposal that inhibition of TGF- $\beta$ -signaling in NK cells, could be a rational strategy for preventing NK cell conversion and restricting tumor metastasis. Multimodal antibodies targeting the receptor TGF- $\beta$ RII and an NK cell-specific receptor, as well as small-molecule inhibitors that prevent the conversion of NK cells into intILC1s or ILC1s, might offer new opportunities for cancer immunotherapy.

## METHODS

Methods, including statements of data availability and any associated accession codes and references, are available in the [online version of the paper](#).

*Note: Any Supplementary Information and Source Data files are available in the online version of the paper.*

## ACKNOWLEDGMENTS

We thank R. Schreiber (Washington University School of Medicine) for MCA1956 fibrosarcoma cells and anti-IFN- $\gamma$  and anti-TNF hybridomas; the animal house and flow cytometry facilities at QIMR Berghofer Medical Research Institute and Walter and Eliza Hall Institute of Medical Research; E. Loza, K. Elder, L. Town, L. Spencer, T. Camilleri and T. Kratina, for mouse breeding, maintenance and genotyping; and K. MacDonald, D. Smith, A. Kallies, L. Beattie, R. Allan, G. Hill and S. Nutt for

discussion, comments and advice on this project. Supported by the National Health and Medical Research Council of Australia (Senior Principal Research Fellowship 1078671 to M.J.S.; Peter Doherty Early Career Fellowship 1088703 to F.S.-F.-G. and 1124690 to T.B.; project grant 1027472 to G.T.B.; Elizabeth Blackburn NHMRC Fellowship to G.T.B.; Independent Research Institute Infrastructure Support scheme grant to G.T.B.; project grants 1066770 & 1057852 N.D.H.; and RD Wright Career development Fellowship 1112113 to N.W.), the Cancer Research Institute Clinical and Laboratory Integration Programs (M.J.S. and N.D.H.), Queensland Institute of Medical Research Berghofer International PhD Scholarship (Y.G. and J.Y.), University of Queensland International Scholarship (Y.G. and J.Y.), the National Breast Cancer Foundation (PF-15-008 to F.S.-F.-G.), Cure Cancer Australia (Priority-Driven Young Investigator Project Grant 1082709 and 1120725 to F.S.-F.-G.), European Molecular Biology Organization (long-term fellowship ALTF 945-2015 to T.B.), the Naito Foundation (K.N.), Cancer Council Queensland (PhD fellowship to A.Y.), Griffith University (PhD scholarships to S.S.N.), Inserm-Avenir-Grant (L.B.), Ligue Nationale Contre le Cancer (L.B.), Fondation ARC Pour la Recherche sur le Cancer (L.B.), the Victorian State Government Operational Infrastructure Scheme (G.T.B.), the Harry J Lloyd Charitable Trust (Melanoma Research Grant to N.D.H.) and the DFG Excellence Cluster Immunosenescence (EXC 1023 to M.H.).

#### AUTHOR CONTRIBUTIONS

Y.G., F.S.-F.-G., T.B., N.D.H., K.N. and M.J.S. designed research, supervised work and wrote the paper; Y.G., F.S.-F.-G., T.B., A.Y., S.F.N., J.R., S.J.B., J.Y., J.S.L., M.M., L.Z., N.D.H., K.N. and M.J.S. performed research; Y.G., F.S.-F.-G., T.B., S.S.N., A.Y., S.F.N., J.R., J.S., N.W., S.J.B., J.Y., M.M., L.Z., M.W.L.T., G.T.B., C.R.E., N.D.H., K.N., M.H. and M.J.S. analyzed data; and L.B., E.V., K.T. and G.T.B. provided experimental materials.

#### COMPETING FINANCIAL INTERESTS

The authors declare competing financial interests: details are available in the [online version of the paper](#).

Reprints and permissions information is available online at <http://www.nature.com/reprints/index.html>. Publisher's note: Springer Nature remains neutral with regard to jurisdictional claims in published maps and institutional affiliations.

- Guillerey, C., Huntington, N.D. & Smyth, M.J. Targeting natural killer cells in cancer immunotherapy. *Nat. Immunol.* **17**, 1025–1036 (2016).
- Yang, L., Pang, Y. & Moses, H.L. TGF-beta and immune cells: an important regulatory axis in the tumor microenvironment and progression. *Trends Immunol.* **31**, 220–227 (2010).
- Wrzesinski, S.H., Wan, Y.Y. & Flavell, R.A. Transforming growth factor- $\beta$  and the immune response: implications for anticancer therapy. *Clin. Cancer Res.* **13**, 5262–5270 (2007).
- Smyth, M.J., Strobl, S.L., Young, H.A., Ortaldo, J.R. & Ochoa, A.C. Regulation of lymphokine-activated killer activity and pore-forming protein gene expression in human peripheral blood CD8<sup>+</sup> T lymphocytes. Inhibition by transforming growth factor-beta. *J. Immunol.* **146**, 3289–3297 (1991).
- Donatelli, S.S. *et al.* TGF- $\beta$ -inducible microRNA-183 silences tumor-associated natural killer cells. *Proc. Natl. Acad. Sci. USA* **111**, 4203–4208 (2014).
- Wilson, E.B. *et al.* Human tumour immune evasion via TGF- $\beta$  blocks NK cell activation but not survival allowing therapeutic restoration of anti-tumour activity. *PLoS One* **6**, e22842 (2011).
- Smyth, M.J. *et al.* CD4<sup>+</sup>CD25<sup>+</sup> T regulatory cells suppress NK cell-mediated immunotherapy of cancer. *J. Immunol.* **176**, 1582–1587 (2006).
- Viel, S. *et al.* TGF- $\beta$  inhibits the activation and functions of NK cells by repressing the mTOR pathway. *Sci. Signal.* **9**, ra19 (2016).
- Sojka, D.K. *et al.* Tissue-resident natural killer (NK) cells are cell lineages distinct from thymic and conventional splenic NK cells. *eLife* **3**, e01659 (2014).
- Constantinides, M.G., McDonald, B.D., Verhoef, P.A. & Bendelac, A. A committed precursor to innate lymphoid cells. *Nature* **508**, 397–401 (2014).
- Fuchs, A. ILC1s in tissue inflammation and infection. *Front. Immunol.* **7**, 104 (2016).
- Robinette, M.L. *et al.* Transcriptional programs define molecular characteristics of innate lymphoid cell classes and subsets. *Nat. Immunol.* **16**, 306–317 (2015).
- Seillet, C. *et al.* Differential requirement for Nfil3 during NK cell development. *J. Immunol.* **192**, 2667–2676 (2014).
- Gasteiger, G., Fan, X., Dikiy, S., Lee, S.Y. & Rudensky, A.Y. Tissue residency of innate lymphoid cells in lymphoid and nonlymphoid organs. *Science* **350**, 981–985 (2015).
- Klose, C.S. *et al.* Differentiation of type 1 ILCs from a common progenitor to all helper-like innate lymphoid cell lineages. *Cell* **157**, 340–356 (2014).
- Spits, H., Bernink, J.H. & Lanier, L. NK cells and type 1 innate lymphoid cells: partners in host defense. *Nat. Immunol.* **17**, 758–764 (2016).
- Seillet, C. & Belz, G.T. Differentiation and diversity of subsets in group 1 innate lymphoid cells. *Int. Immunol.* **28**, 3–11 (2016).
- Vallentin, B. *et al.* Innate Lymphoid Cells in Cancer. *Cancer Immunol. Res.* **3**, 1109–1114 (2015).
- Morvan, M.G. & Lanier, L.L. NK cells and cancer: you can teach innate cells new tricks. *Nat. Rev. Cancer* **16**, 7–19 (2016).
- Cortez, V.S. *et al.* Transforming growth factor- $\beta$  signaling guides the differentiation of innate lymphoid cells in salivary glands. *Immunity* **44**, 1127–1139 (2016).
- Keskin, D.B. *et al.* TGFbeta promotes conversion of CD16<sup>+</sup> peripheral blood NK cells into CD16<sup>-</sup> NK cells with similarities to decidual NK cells. *Proc. Natl. Acad. Sci. USA* **104**, 3378–3383 (2007).
- Narni-Mancinelli, E. *et al.* Fate mapping analysis of lymphoid cells expressing the Nkp46 cell surface receptor. *Proc. Natl. Acad. Sci. USA* **108**, 18324–18329 (2011).
- Ruijtenberg, S. & van den Heuvel, S. Coordinating cell proliferation and differentiation: antagonism between cell cycle regulators and cell type-specific gene expression. *Cell Cycle* **15**, 196–212 (2016).
- Liberzon, A. *et al.* The Molecular Signatures Database (MSigDB) hallmark gene set collection. *Cell Syst.* **1**, 417–425 (2015).
- Smyth, M.J. *et al.* Differential tumor surveillance by natural killer (NK) and NKT cells. *J. Exp. Med.* **191**, 661–668 (2000).
- Smyth, M.J., Crowe, N.Y. & Godfrey, D.I. NK cells and NKT cells collaborate in host protection from methylcholanthrene-induced fibrosarcoma. *Int. Immunol.* **13**, 459–463 (2001).
- Sathe, P. *et al.* Innate immunodeficiency following genetic ablation of Mcl1 in natural killer cells. *Nat. Commun.* **5**, 4539 (2014).
- Knight, D.A. *et al.* Host immunity contributes to the anti-melanoma activity of BRAF inhibitors. *J. Clin. Invest.* **123**, 1371–1381 (2013).
- Krasnova, Y., Putz, E.M., Smyth, M.J. & Souza-Fonseca-Guimaraes, F. Bench to bedside: NK cells and control of metastasis. *Clin. Immunol.* **177**, 50–59 (2017).
- Chaput, N. *et al.* Phase I clinical trial combining imatinib mesylate and IL-2: HLA-DR<sup>+</sup> NK cell levels correlate with disease outcome. *Oncol Immunology* **2**, e23080 (2013).
- Ménard, C. *et al.* Natural killer cell IFN-gamma levels predict long-term survival with imatinib mesylate therapy in gastrointestinal stromal tumor-bearing patients. *Cancer Res.* **69**, 3563–3569 (2009).
- Fuchs, A. *et al.* Intraepithelial type 1 innate lymphoid cells are a unique subset of IL-12- and IL-15-responsive IFN- $\gamma$ -producing cells. *Immunity* **38**, 769–781 (2013).
- Crome, S.Q. *et al.* A distinct innate lymphoid cell population regulates tumor-associated T cells. *Nat. Med.* **23**, 368–375 (2017).
- Dadi, S. *et al.* Cancer immunosurveillance by tissue-resident innate lymphoid cells and innate-like T cells. *Cell* **164**, 365–377 (2016).
- Pikovskaya, O. *et al.* Cutting edge: eomesodermin is sufficient to direct type 1 innate lymphocyte development into the conventional NK lineage. *J. Immunol.* **196**, 1449–1454 (2016).
- Cortez, V.S. *et al.* SMAD4 impedes the conversion of NK cells into ILC1-like cells by curtailing non-canonical TGF- $\beta$  signaling. *Nat. Immunol.* doi:10.1038/ni.3809 (2016).
- Hayakawa, Y. *et al.* IFN-gamma-mediated inhibition of tumor angiogenesis by natural killer T-cell ligand,  $\alpha$ -galactosylceramide. *Blood* **100**, 1728–1733 (2002).
- Ikeda, H., Old, L.J. & Schreiber, R.D. The roles of IFN $\gamma$  in protection against tumor development and cancer immunoeediting. *Cytokine Growth Factor Rev.* **13**, 95–109 (2002).
- Balkwill, F. Tumour necrosis factor and cancer. *Nat. Rev. Cancer* **9**, 361–371 (2009).
- Baluk, P. *et al.* TNF- $\alpha$  drives remodeling of blood vessels and lymphatics in sustained airway inflammation in mice. *J. Clin. Invest.* **119**, 2954–2964 (2009).
- Sainson, R.C. *et al.* TNF primes endothelial cells for angiogenic sprouting by inducing a tip cell phenotype. *Blood* **111**, 4997–5007 (2008).
- Gill, S. *et al.* Rapid development of exhaustion and down-regulation of eomesodermin limit the antitumor activity of adoptively transferred murine natural killer cells. *Blood* **119**, 5758–5768 (2012).
- Doisne, J.M. *et al.* Composition, development, and function of uterine innate lymphoid cells. *J. Immunol.* **195**, 3937–3945 (2015).
- Levi, I. *et al.* Characterization of tumor infiltrating natural killer cell subset. *Oncotarget* **6**, 13835–13843 (2015).
- Bruno, A. *et al.* The proangiogenic phenotype of natural killer cells in patients with non-small cell lung cancer. *Neoplasia* **15**, 133–142 (2013).
- Lima, P.D., Zhang, J., Dunk, C., Lye, S.J. & Croy, B.A. Leukocyte driven-decidual angiogenesis in early pregnancy. *Cell. Mol. Immunol.* **11**, 522–537 (2014).
- Vacca, P. *et al.* Crosstalk between decidual NK and CD14<sup>+</sup> myelomonocytic cells results in induction of Tregs and immunosuppression. *Proc. Natl. Acad. Sci. USA* **107**, 11918–11923 (2010).
- Arteaga, C.L. *et al.* Anti-transforming growth factor (TGF)- $\beta$  antibodies inhibit breast cancer cell tumorigenicity and increase mouse spleen natural killer cell activity. Implications for a possible role of tumor cell/host TGF- $\beta$  interactions in human breast cancer progression. *J. Clin. Invest.* **92**, 2569–2576 (1993).
- Terabe, M. *et al.* Synergistic enhancement of CD8<sup>+</sup> T cell-mediated tumor vaccine efficacy by an anti-transforming growth factor- $\beta$  monoclonal antibody. *Clin. Cancer Res.* **15**, 6560–6569 (2009).
- Morris, J.C. *et al.* Phase I study of GC1008 (fresolimumab): a human anti-transforming growth factor- $\beta$  (TGF $\beta$ ) monoclonal antibody in patients with advanced malignant melanoma or renal cell carcinoma. *PLoS One* **9**, e90353 (2014).
- Akhurst, R.J. & Hata, A. Targeting the TGF $\beta$  signalling pathway in disease. *Nat. Rev. Drug Discov.* **11**, 790–811 (2012).

## ONLINE METHODS

**Mice.** C57BL/6 wild-type, *Rag2<sup>-/-</sup>γc<sup>-/-</sup>* and *Ptprc<sup>a</sup>* (CD45.1<sup>+</sup>) mice were either purchased from the Walter and Eliza Hall Institute for Medical Research (WEHI) or obtained from QIMR Berghofer Medical Research Institute (QIMR). C57BL/6 *Ncr1<sup>cre/wt</sup>* mice<sup>22</sup>, *Ncr1<sup>cre/wt</sup>TgfbR1CA<sup>fl/fl</sup>* mice<sup>52</sup>, *Ncr1<sup>cre/wt</sup>TgfbRII<sup>fl/fl</sup>* mice<sup>8</sup>, *Ncr1<sup>cre/wt</sup>Mcl1<sup>fl/fl</sup>* mice<sup>27</sup> and Eomes-mCherry reporter mice<sup>53</sup> were described before. All mice were bred and maintained at QIMR and/or WEHI. All animal experiments were performed using age- and sex-matched cohorts of mice (age range of 6–12 weeks). Cohort sizes are described in each figure legend and were based on historical controls to achieve statistical significance. No mice were excluded based on pre-established criteria. Cohorts of mice treated with indicated antibodies were allocated randomly. All experiments were approved by QIMR and WEHI Animal Ethics Committees.

**Cell lines.** SM1WT1 melanoma cells<sup>28</sup> and MCA1956 fibrosarcoma cells (provided by R. Schreiber, Washington University School of Medicine) were cultured at 37 °C in RPMI-1640 medium supplemented with 10% FCS, 1% GlutaMAX (Gibco), 10 mM HEPES (Sigma-Aldrich), 1% penicillin/streptomycin (Gibco). B16F10 melanoma cells (obtained from ATCC), RM-1 prostate cancer cells<sup>8</sup>, E0771-LMB mCherry<sup>+</sup> breast cancer cells<sup>54</sup> were cultured 37 °C in DMEM (Gibco) supplemented with 10% FCS, 1% GlutaMAX, 10 mM HEPES and 1% penicillin-streptomycin. RM-1 cells were maintained in 10% CO<sub>2</sub>, while all other cell lines were maintained in 5% CO<sub>2</sub>. All cell lines were tested and found to be mycoplasma negative.

**In vivo tumor models.** *In vivo* tumor models were performed as previously described<sup>28,55–57</sup>. For MCA-carcinogen-induced fibrosarcoma, male mice of the appropriate genotype and the respective wild-type control mice were given subcutaneous injection of 25 μg or 300 μg MCA (Sigma-Aldrich) dissolved in corn oil and were monitored over the course of 250 d for fibrosarcoma development. Tumor with a diameter of over 3 mm and progressive growth were recorded as positive. Some groups of wild-type mice received intraperitoneal injection of 50 μg of either control antibody (polyclonal rabbit IgG, BioXcell, CAT#BE0095) or anti-asGM1 (CAT# 986-10001, Wako Chemicals USA Inc) weekly for the first 56 d after injection of MCA, unless specified otherwise. For the primary SM1WT1 melanoma and MCA1956 fibrosarcoma models, 1 × 10<sup>6</sup> SM1WT1 or MCA1956 cancer cells in 100 μl PBS were injected subcutaneously at day 0 into the appropriate transgenic mice. Only male mice were used for SM1WT1 tumor model, whereas both males and females were used for MCA1956 tumor model. Tumor size (mm<sup>2</sup>) was calculated as the product of two diameters (length × width) of each tumor. In some experiments, 250 μg anti-IFN-γ (H22) or anti-TNF (TN319.12) (hybridomas provided by R. Schreiber (Washington University School of Medicine)) or the IgG control antibody (BE0260, Bio X Cell) were injected intraperitoneally on day 10, 12, 18 and 20; 50 μg anti-asGM1 or control IgG (both identified above) were injected intraperitoneally on days –1, 0, 7, 14 and 21, unless specified otherwise. For experimental lung metastasis models, B16F10 cells (5 × 10<sup>3</sup>, 10<sup>4</sup> or 10<sup>5</sup> cells per male mouse), mCherry<sup>+</sup> E0771-LMB cells (3.5 × 10<sup>5</sup> cells per female mouse) or RM-1 cells (2 × 10<sup>5</sup> cells per male mouse) were injected intravenously into the tail vein of transgenic mice and their respective controls. For the metastasis model, some mice were given injection of 250 μg anti-IFN-γ, anti-TNF or control IgG (all identified above) on days –1, 0 and 7. Lungs were harvested 14 d after tumor injection. B16F10 or RM-1 macrometastatic nodules were counted under a dissection microscope, while E0771-LMB metastases were quantified by measurement of mCherry fluorescence from excised lungs (IVIS Spectrum, Perkin Elmer) and by detection of the abundance of expression of the gene encoding mCherry (present only in tumor cells) relative to that of the gene encoding vimentin (present in all cells) by duplex qPCR, as previously described<sup>58</sup>.

**Flow cytometry.** Mice were killed and organs were harvested and prepared for flow cytometry as previously described<sup>55,59</sup>. For liver and tumor samples, lymphocytes were enriched using 37.5% Percoll solution (GE Healthcare). Single-cell suspensions from various organs were incubated on ice for 15 min in Fc blocking buffer (PBS containing 2% FBS and anti-CD16/32 (clone 2.4G2; hybridoma obtained from ATCC)). Reagents or antibodies targeting the following epitopes were purchased from BioLegend: 7-AAD, CD3

(145-2C11), CD19 (6D5), CD49b (DX5 and HMα2), CD62L (MEL-14), CD96 (3.3), DNAM-1 (10E5), IFN-γ (XMGI.2), NK1.1 (PK136), NKp46 (29A1.4), TIGIT (1G9), TCRβ (H57-597), TNF (MP6-XT220) and Zombie Yellow Fixable Viability Kit. Reagents or antibodies targeting the following epitopes were purchased from eBioscience: CD45.1 (A20), CD45.2 (104), CD49b (DX5), CTLA-4 (UC10-4B9), Eomes (Dan1Imag), LAG-3 (eBioC9B7W), TIM-3 (RMT3-23), TCRβ (H57-597) and TRAIL (N2B2). Reagents or antibodies targeting the following epitopes were purchased from BD Biosciences: CD49a (Ha31/8), NK1.1 (PK136), PD-1 (J43), Ki67 (B56) and Fixable Viability Stain 520 or 700. Antibodies targeting CD45.2 (104-2), CD49a (REA493) and CD69 (H1.2F3) were purchased from Miltenyi Biotec. Cell number was calculated by using BD Liquid Counting Beads (BD Biosciences). A lineage (Lin) cocktail consisting of antibodies to CD3, CD19 and TCRβ (all identified above) was used for lineage-cell exclusion where indicated. For intracellular cytokine detection, lymphocyte-enriched tumor homogenates were incubated in RPMI-1640 supplemented with 10% FCS, Cell Stimulation Cocktail plus protein transport inhibitors (stimulated cells) (eBioscience), or GolgiStop and GolgiPlug (unstimulated control cells) (both from BD Biosciences) at 37 °C for 4 h. After cell-surface staining, samples were fixed and permeabilized using Intracellular Fixation & Permeabilization Buffer Set (eBioscience), and stained with antibodies in 1 × Permeabilization Buffer. Data acquisition was performed using LSRFortessa Flow Cytometer (BD Biosciences). Flow cytometry was performed using Flowjo (Treestar) software.

**Cell sorting.** NK cells (7-AAD<sup>-</sup>Lin<sup>-</sup>CD45<sup>+</sup>NK1.1<sup>+</sup>NKp46<sup>+</sup>CD49a<sup>-</sup>CD49b<sup>+</sup>), intILC1s (7-AAD<sup>-</sup>Lin<sup>-</sup>CD45<sup>+</sup>NK1.1<sup>+</sup>NKp46<sup>+</sup>CD49a<sup>+</sup>CD49b<sup>+</sup>) and ILC1s (7-AAD<sup>-</sup>Lin<sup>-</sup>CD45<sup>+</sup>NK1.1<sup>+</sup>NKp46<sup>+</sup>CD49a<sup>+</sup>CD49b<sup>-</sup>) from various organs of transgenic or wild-type mice were sorted by a BD FACSAria II cell sorter (BD Biosciences). In certain experiments, mCherry was used to distinguish NK cells (Eomes<sup>+</sup>) from ILC1s (Eomes<sup>-</sup>) for samples obtained from Eomes-mCherry reporter mice. For liver and tumor samples, lymphocytes were enriched by using 37.5% Percoll solution (GE Healthcare). For spleen, liver and tumor samples, group 1 ILCs were further enriched by the NK Cell Isolation Kit II using autoMACS Pro Separator (both from Miltenyi Biotec), before antibody staining and cell sorting.

**In vitro group 1 ILC culture.** For NK cell or ILC1 *in vitro* culture, freshly sorted liver NK cells or ILC1s, labeled with the division-tracking dye CFSE (BioLegend), were plated at a density of 25,000 cells per well in 96-well plates (Greiner Bio-One) containing RPMI-1640 supplemented with 10% FCS, 1% non-essential amino acids (Gibco), 1% sodium pyruvate (Gibco), 10 mM HEPES, 1% GlutaMAX, 0.1% 2-mercaptoethanol (Gibco) and 1% penicillin-streptomycin in the presence of rIL-15, rIL-15-IL-15Rα complex or TGF-β1 (all from eBioscience) at the appropriate concentrations at 37 °C 5% CO<sub>2</sub> for 5 d. For intILC1 and NK cell *in vitro* culture, sorted intILC1s and NK cells from pooled spleens of *RI<sup>CA-FL</sup>* or *RI<sup>CA-WT</sup>* mice were cultured in serum-free TexMACS medium (Miltenyi Biotec) supplemented with 1% Glutamax, 0.1% 2-mercaptoethanol, 1% non-essential amino acids, 1% sodium pyruvate, 1% penicillin-streptomycin and 50 ng/ml rIL-15 at 37 °C 5% CO<sub>2</sub> for 4 d.

**RNA sequencing and bioinformatics analysis.** Tumor ILC1s, intILC1s and NK cells were sorted from MCA1956 tumors harvested from male wild-type mice. Total RNA was extracted using RNeasy Mini Kit (Qiagen). A cDNA library was generated using a SMARTer Universal Low Input RNA Kit (Clontech) and a TruSeq RNA Library Prep Kit v2 (Illumina). Samples were sequenced on a HiSeq 2500 System (Illumina) by 100-bp paired-end sequencing. The R/Bioconductor computing platform was used for RNA-seq analyses. FASTQ files containing RNA-seq raw reads of tumor NK cells, intILC1s and ILC1s were aligned to the mm10 mouse reference genome using the Rsubread aligner<sup>60</sup>. RNA-seq data of liver and spleen NK and ILC1 cells were downloaded from the GEO sequencing read archive (GSE52047)<sup>9</sup>. The log<sub>2</sub> transformation, normalization and normal linear modeling of the aligned read count matrix were done with the voom algorithm implemented in the limma package, which makes the limma empirical Bayes analysis pipeline accessible to RNA-seq read count data<sup>61,62</sup>. Differentially expressed genes were identified by empirical Bayes moderated *t*-tests, and *P* values were corrected for multiple testing by the Benjamini & Hochberg method (FDR). Genes expressed differentially by tumor NK cells and tumor

ILC1s were defined by an absolute change in expression of over onefold ( $\log_2$  values) and a FDR of  $< 0.01$ . For gene-set-enrichment analysis (GSEA), the  $t$ -test statistics was used as ranked metric for the GSEA pre-ranked gene list algorithm<sup>63</sup>. GSEA software was downloaded from the GSEA homepage of the Broad institute (<http://software.broadinstitute.org/gsea/index.jsp>). The curated hallmark gene set collection of the Molecular Signature Database (MSigDB version 5.0) was used for GSEA<sup>24</sup>. Core enrichment genes were used to assess hallmark gene signature expression in individual samples. Combined  $z$ -scores were calculated as described<sup>64</sup>. Classical multidimensional scaling was performed with the R function `cmdscale` with euclidean distance matrix as input. For this purpose, the voom processed gene expression matrix of tumor NK cells, intILC1s and ILC1s was size-reduced by a variance cut-off of 0.5 and transformed into an euclidean distance matrix by the R function `dist`. A phylogenetic tree plot (ape R package) was generated based on the DIANA divisive hierarchical clustering method from the cluster R package.

**Adoptive-transfer assays of group 1 ILC subsets.** Freshly sorted NK cells or intILC1s from pooled spleens of wild-type or transgenic mice were injected intravenously into *Rag2*<sup>-/-</sup>*γc*<sup>-/-</sup> recipient mice ( $5 \times 10^5$  cells per mouse). Liver group 1 ILCs in recipient mice were assessed by flow cytometry 7, 14 or 21 d after reconstitution. For assessment of NK cell plasticity in tumors, NK cells sorted from pooled spleens of the appropriate transgenic mice were injected intravenously into MCA1956-tumor-bearing *Rag2*<sup>-/-</sup>*γc*<sup>-/-</sup> mice ( $5 \times 10^5$  NK cells per mouse). Tumors were harvested 16 d after NK cell reconstitution. For some experiments, sorted NK cells were injected intratumorally into MCA1956-tumor-bearing *Ptprc*<sup>a</sup> (CD45.1<sup>+</sup>) mice at a dose of  $3 \times 10^5$  to  $5 \times 10^5$  NK cells in 50  $\mu$ l PBS per mouse. Tumors were harvested 4 or 7 d after intratumoral injection of NK cells.

**Multiplex assay.** Sorted NK cells, intILC1s and ILC1s from MCA1956 tumors were seeded at 20,000 cells per well in a 96-well plate. Cells were cultured in complete DMEM medium (total 50  $\mu$ l per well) in presence of 25 ng/ml PMA and 500 ng/ml ionomycin at 37 °C for 16 h. Cytokines and chemokines in the supernatant were determined by Cytometric Bead Array (BD Biosciences). Data were analyzed on FCAP Array Software (BD Biosciences).

**ELISA.** Sorted NK cells, intILC1s and ILC1s from MCA1956 tumors were seeded at 20,000 cells per well in a 96-well plate. Cells were cultured in complete DMEM medium (total 50  $\mu$ l per well) in presence of 25 ng/ml PMA and 500 ng/ml ionomycin at 37 °C for 16 h. PDGF-AB in the supernatant was determined by a Quantikine PDGF-AB ELISA kit (R&D Systems) following manufacturer's instruction. Data were acquired on a microplate reader (BioTek).

**Tube-formation assay.** Matrigel (BD Biosciences) was used to coat 96-well plates, with 50  $\mu$ l Matrigel (10 mg/ml). Plates were incubated for 30 min at 37 °C. 20,000 brain endothelial cells (bEND.5) were seeded into each well in serum-free DMEM medium and stimulated with supernatants from PMA- and ionomycin-activated NK cells, intILC1s and ILC1s isolated from MCA1956 tumors. Images of endothelial cell cultures were acquired on an Olympus IX81 imaging system. bEND.5 cells were cultured as described previously<sup>65</sup>.

**Human samples.** The translational research study of specimens from patients with GISTs and healthy volunteers was approved by the local Ethic Committee

(2007-A00923-50), and all patients signed a written informed consent for participation. Antibodies targeting the following human epitopes were purchased from BioLegend: CD3 (OKT3), CD16 (3G8), CD45 (J.33), CD56 (N901) and CXCR6 (K041E5). Antibodies targeting the following human epitopes were purchased from BD Biosciences: CD19 (HIB19) and CD14 (M5E2). Dead cells were excluded using the Live/Dead Fixable Yellow dead cell stain kit (Life Technologies). Cell samples were acquired on a BD FACSCanto II flow cytometer with single-stained antibody-capturing beads used for compensation (Compbeads, BD Biosciences or UltraComp eBeads, eBioscience). Data were analyzed with BD FACSDiva software.

**Statistical analysis.** Statistical analyses were performed using GraphPad Prism Software. A Mann-Whitney  $U$ -test, unpaired two-sided  $t$ -test, pairwise two-sided  $t$ -tests with Benjamini & Hochberg (FDR) correction for multiple testing and one-way ANOVA with Tukey's multiple comparison test were used for comparison of two or more groups. A log-rank test was used for evaluation of differences in tumor free percentages. Linear regression analysis was used for investigating correlations of cell percentages and tumor weight.  $P < 0.05$  was considered statistically significant.

A Life Sciences Reporting Summary for this paper is available online.

**Data availability.** The data that support the findings of this study are available from the corresponding author upon request. RNA sequencing data have been deposited in the European Genome-phenome Archive (EGA) with accession code EGA00001002514.

52. Viant, C. *et al.* Transforming growth factor- $\beta$  and Notch ligands act as opposing environmental cues in regulating the plasticity of type 3 innate lymphoid cells. *Sci. Signal.* **9**, ra46 (2016).
53. Kara, E.E. *et al.* CCR2 defines *in vivo* development and homing of IL-23-driven GM-CSF-producing Th17 cells. *Nat. Commun.* **6**, 8644 (2015).
54. Johnstone, C.N. *et al.* Functional and molecular characterisation of E0771.LMB tumours, a new C57BL/6-mouse-derived model of spontaneously metastatic mammary cancer. *Dis. Model. Mech.* **8**, 237–251 (2015).
55. Blake, S.J. *et al.* Suppression of metastases using a new lymphocyte checkpoint target for cancer immunotherapy. *Cancer Discov.* **6**, 446–459 (2016).
56. Souza-Fonseca-Guimaraes, F. *et al.* NK cells require IL-28R for optimal *in vivo* activity. *Proc. Natl. Acad. Sci. USA* **112**, E2376–E2384 (2015).
57. Delconte, R.B. *et al.* CIS is a potent checkpoint in NK cell-mediated tumor immunity. *Nat. Immunol.* **17**, 816–824 (2016).
58. Rautela, J. *et al.* Loss of Host Type-I IFN signaling accelerates metastasis and impairs NK-cell antitumor function in multiple models of breast cancer. *Cancer Immunol. Res.* **3**, 1207–1217 (2015).
59. Ngiew, S.F. *et al.* A threshold level of intratumor CD8<sup>+</sup> T-cell PD1 expression dictates therapeutic response to anti-PD1. *Cancer Res.* **75**, 3800–3811 (2015).
60. Liao, Y., Smyth, G.K. & Shi, W. The Subread aligner: fast, accurate and scalable read mapping by seed-and-vote. *Nucleic Acids Res.* **41**, e108 (2013).
61. Law, C.W., Chen, Y., Shi, W. & Smyth, G.K. voom: Precision weights unlock linear model analysis tools for RNA-seq read counts. *Genome Biol.* **15**, R29 (2014).
62. Ritchie, M.E. *et al.* limma powers differential expression analyses for RNA-sequencing and microarray studies. *Nucleic Acids Res.* **43**, e47 (2015).
63. Subramanian, A. *et al.* Gene set enrichment analysis: a knowledge-based approach for interpreting genome-wide expression profiles. *Proc. Natl. Acad. Sci. USA* **102**, 15545–15550 (2005).
64. Lee, E., Chuang, H.Y., Kim, J.W., Ideker, T. & Lee, D. Inferring pathway activity toward precise disease classification. *PLoS Comput. Biol.* **4**, e1000217 (2008).
65. Bald, T. *et al.* Ultraviolet-radiation-induced inflammation promotes angiogenesis and metastasis in melanoma. *Nature* **507**, 109–113 (2014).

## Life Sciences Reporting Summary

Nature Research wishes to improve the reproducibility of the work that we publish. This form is intended for publication with all accepted life science papers and provides structure for consistency and transparency in reporting. Every life science submission will use this form; some list items might not apply to an individual manuscript, but all fields must be completed for clarity.

For further information on the points included in this form, see [Reporting Life Sciences Research](#). For further information on Nature Research policies, including our [data availability policy](#), see [Authors & Referees](#) and the [Editorial Policy Checklist](#).

### ► Experimental design

#### 1. Sample size

Describe how sample size was determined.

Mouse group numbers described in the legends were based on availability and historical controls to achieve statistical significance.

#### 2. Data exclusions

Describe any data exclusions.

No mice were excluded based on pre-established criteria.

#### 3. Replication

Describe whether the experimental findings were reliably reproduced.

All experimental repeats were successful.

#### 4. Randomization

Describe how samples/organisms/participants were allocated into experimental groups.

No active randomization was applied to experimental groups. The majority of sample/animal groups were defined by mouse strain or experimental treatment.

#### 5. Blinding

Describe whether the investigators were blinded to group allocation during data collection and/or analysis.

None of our experiments were performed in a blinded fashion.

Note: all studies involving animals and/or human research participants must disclose whether blinding and randomization were used.

#### 6. Statistical parameters

For all figures and tables that use statistical methods, confirm that the following items are present in relevant figure legends (or in the Methods section if additional space is needed).

n/a Confirmed

- The exact sample size ( $n$ ) for each experimental group/condition, given as a discrete number and unit of measurement (animals, litters, cultures, etc.)
- A description of how samples were collected, noting whether measurements were taken from distinct samples or whether the same sample was measured repeatedly
- A statement indicating how many times each experiment was replicated
- The statistical test(s) used and whether they are one- or two-sided (note: only common tests should be described solely by name; more complex techniques should be described in the Methods section)
- A description of any assumptions or corrections, such as an adjustment for multiple comparisons
- The test results (e.g.  $P$  values) given as exact values whenever possible and with confidence intervals noted
- A clear description of statistics including central tendency (e.g. median, mean) and variation (e.g. standard deviation, interquartile range)
- Clearly defined error bars

See the web collection on [statistics for biologists](#) for further resources and guidance.

## ► Software

Policy information about [availability of computer code](#)

### 7. Software

Describe the software used to analyze the data in this study.

Flowjo v10 and BD FACSDiva were used for flow cytometry analysis. FCAP Array was used to analyze data generated by multiplex assay. GraphPad Prism 7 was used for statistical analysis. R was used for RNA sequencing analysis. Computer code used in this study was previously described and is freely available. Reference provided in Methods.

For manuscripts utilizing custom algorithms or software that are central to the paper but not yet described in the published literature, software must be made available to editors and reviewers upon request. We strongly encourage code deposition in a community repository (e.g. GitHub). *Nature Methods* [guidance for providing algorithms and software for publication](#) provides further information on this topic.

## ► Materials and reagents

Policy information about [availability of materials](#)

### 8. Materials availability

Indicate whether there are restrictions on availability of unique materials or if these materials are only available for distribution by a for-profit company.

N/A

### 9. Antibodies

Describe the antibodies used and how they were validated for use in the system under study (i.e. assay and species).

The clones and suppliers of all antibodies used were described in the "Flow cytometry" and "Human samples" of Method.

### 10. Eukaryotic cell lines

a. State the source of each eukaryotic cell line used.

Please refer to the "Cell lines" section of Methods for further detail. References were provided.

b. Describe the method of cell line authentication used.

All cell lines used were as referenced in the "Cell lines" section of Methods.

c. Report whether the cell lines were tested for mycoplasma contamination.

All cell lines were tested mycoplasma negative.

d. If any of the cell lines used are listed in the database of commonly misidentified cell lines maintained by [ICLAC](#), provide a scientific rationale for their use.

N/A

## ► Animals and human research participants

Policy information about [studies involving animals](#); when reporting animal research, follow the [ARRIVE guidelines](#)

### 11. Description of research animals

Provide details on animals and/or animal-derived materials used in the study.

Methods summary. Paragraph 'mice'.

Policy information about [studies involving human research participants](#)

### 12. Description of human research participants

Describe the covariate-relevant population characteristics of the human research participants.

GIST samples were provided by Gustave Roussy Institute (Villejuif, France), European Hospital Georges Pompidou (Paris, France), Institut Mutualiste Montsouris (Paris, France) and Hospital Jean Minjoz (Besançon, France). The study was approved by the local ethical committee (2007-A00923-50) and informed written consent was obtained from patients. PBMCs of Healthy Volunteer (HV) were obtained from buffy coat provided by the Etablissement Français du Sang (EFS, Créteil, France).